



Benchmarking of Data-Driven Causality Discovery Approaches in the Interactions of Arctic Sea Ice and Atmosphere

OPEN ACCESS

Edited by:

Justin Sheffield, University of Southampton, United Kingdom

Reviewed by:

Zachary Langford,
Oak Ridge National Laboratory (DOE),
United States
James Overland,
National Oceanic and Atmospheric
Administration (NOAA), United States
Michel Tsamados,
University College London,
United Kingdom

*Correspondence:

Jianwu Wang jianwu@umbc.edu

[†]Present address:

Matthäus Kleindessner, Amazon, Tubingen, Germany

Specialty section:

This article was submitted to Data-driven Climate Sciences, a section of the journal Frontiers in Big Data

Received: 15 December 2020 Accepted: 02 August 2021 Published: 24 August 2021

Citation:

Huang Y, Kleindessner M, Munishkin A, Varshney D, Guo P and Wang J (2021) Benchmarking of Data-Driven Causality Discovery Approaches in the Interactions of Arctic Sea Ice and Atmosphere. Front. Big Data 4:642182. doi: 10.3389/fdata.2021.642182 Yiyi Huang¹, Matthäus Kleindessner^{2†}, Alexey Munishkin³, Debvrat Varshney⁴, Pei Guo⁴ and Jianwu Wang^{4*}

¹Department of Hydrology and Atmospheric Sciences, University of Arizona, Tucson, AZ, United States, ²Paul G. Allen School of Computer Science and Engineering, University of Washington, Seattle, WA, United States, ³Department of Computer Science and Engineering, University of California Santa Cruz, Santa Cruz, CA, United States, ⁴Department of Information Systems, University of Maryland, Baltimore, MD, United States

The Arctic sea ice has retreated rapidly in the past few decades, which is believed to be driven by various dynamic and thermodynamic processes in the atmosphere. The newly open water resulted from sea ice decline in turn exerts large influence on the atmosphere. Therefore, this study aims to investigate the causality between multiple atmospheric processes and sea ice variations using three distinct data-driven causality approaches that have been proposed recently: Temporal Causality Discovery Framework Noncombinatorial Optimization via Trace Exponential and Augmented lagrangian for Structure learning (NOTEARS) and Directed Acyclic Graph-Graph Neural Networks (DAG-GNN). We apply these three algorithms to 39 years of historical time-series data sets, which include 11 atmospheric variables from ERA-5 reanalysis product and passive microwave satellite retrieved sea ice extent. By comparing the causality graph results of these approaches with what we summarized from the literature, it shows that the static graphs produced by NOTEARS and DAG-GNN are relatively reasonable. The results from NOTEARS indicate that relative humidity and precipitation dominate sea ice changes among all variables, while the results from DAG-GNN suggest that the horizontal and meridional wind are more important for driving sea ice variations. However, both approaches produce some unrealistic cause-effect relationships. Additionally, these three methods cannot well detect the delayed impact of one variable on another in the Arctic. It also turns out that the results are rather sensitive to the choice of hyperparameters of the three methods. As a pioneer study, this work paves the way to disentangle the complex causal relationships in the Earth system, by taking the advantage of cutting-edge Artificial Intelligence technologies.

Keywords: causality discovery, time series, arctic sea ice, temporal causality discovery framework, noncombinatorial optimization *via* trace exponential and augmented lagrangian for structure learning, directed acyclic graph-graph neural networks, atmosphere-sea ice interactions

1

1 INTRODUCTION

Warming in the Arctic has been much faster than in the rest of the world in both observations and model simulations, a phenomenon known as the Arctic amplification (Holland and Bitz, 2003; Serreze and Barry, 2011). Decline in sea ice has occurred in all seasons, which is believed to be the major driver of Arctic amplification. Over the last few decades, Arctic summer sea ice extent has declined by nearly 50% with accelerated retreat in the early 21st century (Serreze and Stroeve, 2015; Simmonds, 2015). These dramatic changes in the Arctic sea ice affect a growing community of diverse stakeholders. Accompanying this growing interest is an urgent demand to increase the pace and scope of the advancements in physical understanding and predictive capabilities. As one of the most important components in the Earth System, the atmosphere actively interacts with the sea ice underneath. On the one hand, the sea ice variations are caused by different dynamic and thermodynamic forcings. On the other hand, sea ice decline in turn exerts large influence on the atmosphere. This will further alter the climate patterns in both Arctic and mid-latitudes, which results in more frequent extreme weather events (Cohen et al., 2014; Simmonds and Govekar, 2014; Sun et al., 2016; Yao et al., 2017; Luo et al., 2018; Luo et al., 2019a; Luo et al., 2019b). These two-way feedbacks are potentially very important in terms of understanding the Arctic warming in the past and future. In most cases, these connections are highly nonlinear and conditionally constrained (e.g., differ by season or region), making them even more complex. For example, a link between recent winter sea ice decline and mid-latitude cold extremes could be mediated by whether there is a weak gradient of background potential vorticity (Luo et al., 2019b; Luo et al., 2018; Luo et al., 2019a). Therefore, it is vital to analyze both the sea ice retreat's influence on the atmosphere and vice versa.

The traditional way to discover causal relations is to manipulate the value of a variable by using interventions or real-life experiments. All other influencing factors of the target variable can be held fixed, to test whether a manipulation of a potential cause changes the target variable (Nauta et al., 2019). Specifically, the typical approach for assessing causal links in climate study is targeted modeling experiments. Such experiments are often computationally expensive, time-consuming, or even impossible to carry out. More importantly, the large biases and substantial model spread remain in the state-of-the-art climate models (Stocker et al., 2013), which further introduce some unrealistic causal relations. With the current advances in digital sensing and data assimilation, we have entered a period where Earth science tends to be data rich in observations (Overpeck et al., 2011), allowing us to do data-driven causality discovery (Guo et al., 2020; Zhang et al., 2018; Nauta et al., 2019). The data-driven causality approach aids scientists in identifying and extracting signals by analyzing statistical properties of purely observational data, which augments targeted model studies and has direct ties to forecasting and prediction. For time-series data, many popular data-driven causality frameworks are proposed such as Granger Causality (Granger, 1969), PC Momentary Conditional Independence (PCMCI) (Runge et al., 2019), Time Series Models with Independent Noise (TiMINo) (Peters et al., 2012), Additive Non-linear Time Series Model (ANLTSM) (Chu and Glymour, 2008) and time series Fast Causal Inference (tsFCI) (Entner and Hoyer, 2010). Several different frameworks for observational analysis have been applied to climate science to provide graphical representations of causal relations. For example, Ebert-Uphoff and Deng (2012) investigated causal relationships between four prominent modes of atmospheric low-frequency variability in boreal winter using Graphic Models. McGraw and Barnes (2018) highlighted the Granger Causality by a simple Monte Carlo example. More recently, Song et al. (2018), Song et al. (2019) demonstrated the Granger causality between El Niño and the southern oscillation (ENSO) and other climate variables. Some other applications in climate sciences include Chu et al. (2005); Zerenner et al. (2014); Hussung et al. (2019). Among them, the most relevant topic is the connections between Arctic and mid-latitude climate patterns, such as the Arctic drivers of mid-latitude winter circulations (Kretschmer et al., 2016; Samarasinghe et al., 2019) as well as the impacts of Arctic sea ice on circulations in the North Atlantic Ocean (Strong et al., 2009) and Western Pacific (Matthewman and Magnusdottir, 2011). However, neither study investigates the relationship between sea ice retreat and the atmospheric dynamic and thermodynamic processes in the Arctic only, which is the focus of this study. It is unclear whether different causality approaches would produce similar results, or whether a particular technique is best suited for this topic as each study employs a different approach. Moreover, it is also valuable to evaluate whether these data-driven causality discovery approaches could capture those conditional and threshold-related connections.

Thus, the overarching goal of this study is to investigate the causality between multiple atmospheric processes and sea ice variations from sub-seasonal to seasonal timescales using datadriven causality approaches. Instead of performing multiple climate model simulations, here we focus solely on an observational-type analysis. Specifically, three distinct datadriven causality approaches, Temporal Causality Discovery Framework (TCDF) (Nauta et al., 2019), Non-combinatorial Optimization via Trace Exponential and Augmented lagrangian for Structure learning (NOTEARS) (Zheng et al., 2018) and Directed Acyclic Graph-Graph Neural Networks (DAG-GNN) (Yu et al., 2019), will be used and compared to determine whether they are suitable for the particular climate study. The main reasons we chose these three approaches are: 1) the three approaches are relatively new (published in 2018 or later) and we have not seen studies applying or evaluating them with climate data; 2) both TCDF and DAG-GNN are deep learning based approaches and deep learning approaches normally can learn nonlinearity from datasets better than traditional machine learning approaches (Schmidhuber, 2015). Because DAG-GNN is built on top of NOTEARS for nonlinearity mapping, we included NOTEARS to see whether DAG-GNN can do better than NOTEARS for our dataset.

This paper is structured in the following sections. Section 2 summarizes the main conclusions from previous studies in terms of causal relations between different atmospheric processes and Arctic sea ice variations; Section 3 lists data sets and data preprocessing methods and steps; Section 4 introduces three data-driven causality discovery frameworks; Section 5 summarizes the results generated by each method and compares those results with

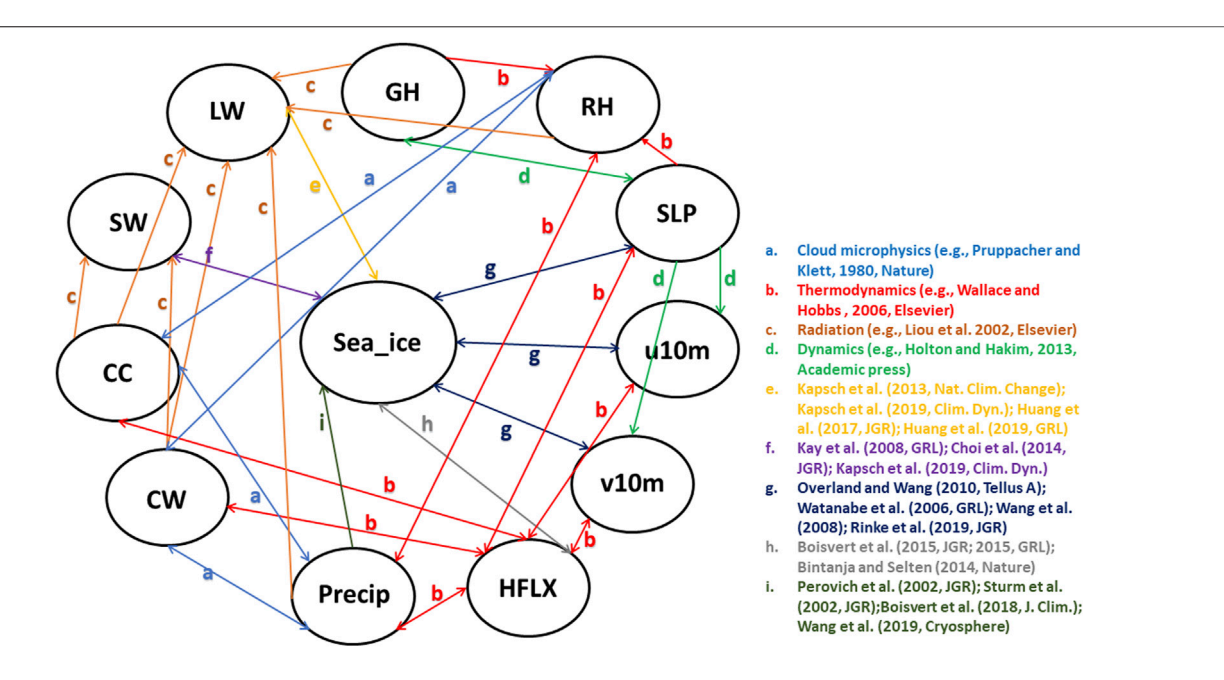


FIGURE 1 The causality graph between key atmospheric variables and sea ice over the Arctic based on literature review. This graph represents the domain knowledge. Note that the processes a-d are well-known atmospheric processes, which can be summarized from multiple textbooks. The processes e-i are summarized from recent peer-reviewed publications and they are ongoing research. The sea_ice here represents sea ice coverage and/or sea ice thickness; GH is the geopotential height; RH is relative humidity; SLP means sea level pressure; u10m and v10m represents meridional and zonal wind at u10m respectively; u10m and u10m represents meridional and zonal wind at u10m represent net shortwave and longwave flux at the surface, respectively.

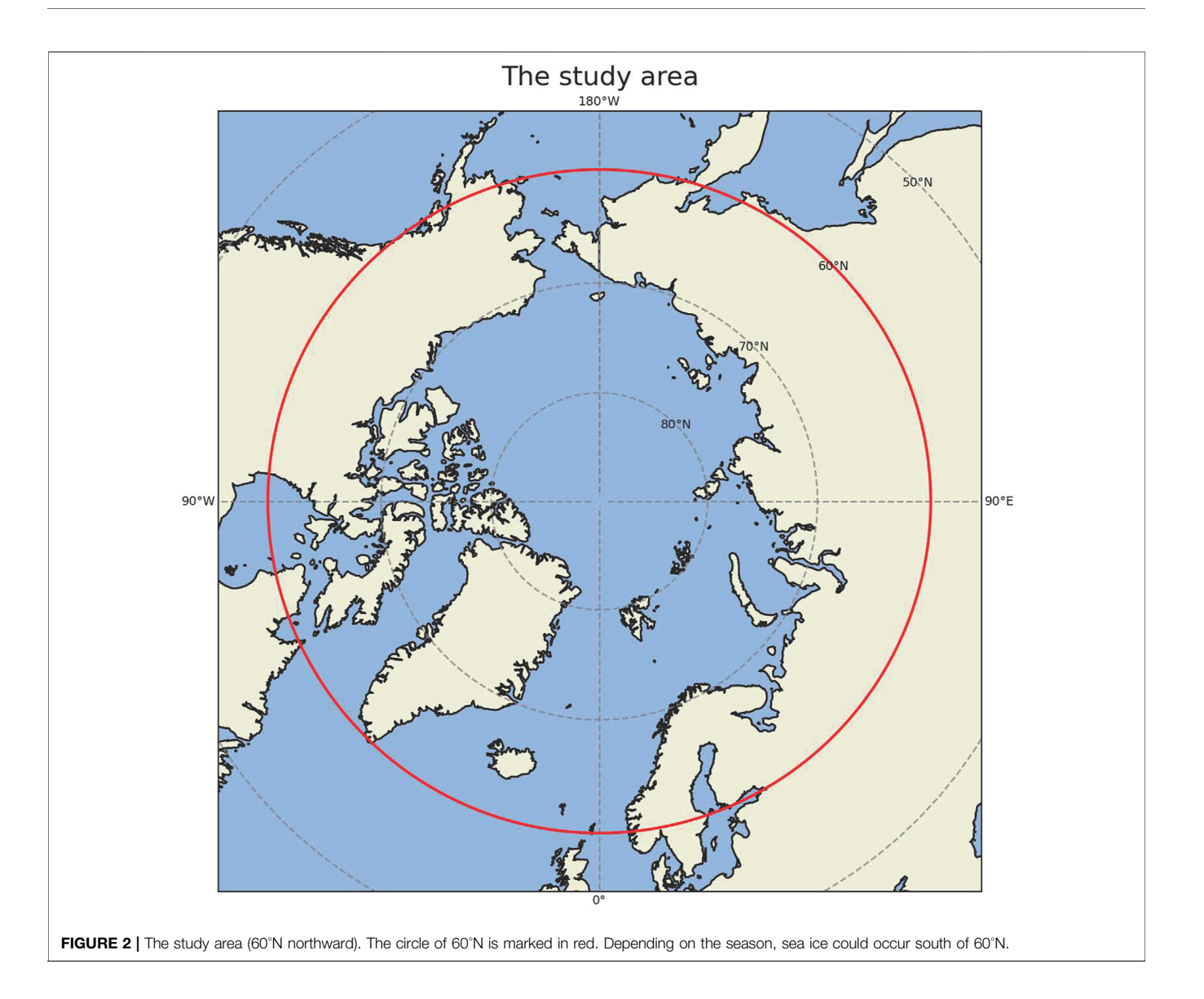
a causality graph based on literature review. Finally, **Section 6** reports the main conclusions and limitations of this study.

2 CAUSALITY BETWEEN ATMOSPHERIC PROCESSES AND ARCTIC SEA ICE VARIATIONS

Due to the two-way interactions between the atmosphere and sea ice, studying causality between them is a challenging but important task, which makes it an area of high interest within polar climate community. The sea ice variations can be caused by different dynamical and thermodynamical processes. Important dynamical processes include anomalous surface wind (Spreen et al., 2011; Wu et al., 2012), regional atmospheric circulation patterns (Overland and Wang, 2010; Screen et al., 2018; Rinke et al., 2019) and abnormal storm activities (Simmonds et al., 2008; Simmonds and Keay, 2009; Screen et al., 2011; Simmonds and Rudeva, 2012; Parkinson and Comiso, 2013; Simmonds and Rudeva, 2014). Cloud (Kapsch et al., 2013), radiation (Kay and Gettelman, 2009; Choi et al., 2014) and precipitation (Boisvert et al., 2018; Wang et al., 2019; Marcovecchio et al., 2021) are the important thermodynamic factors controlling Arctic sea ice trends and variability. On the other hand, sea ice decline in turn exerts large influence on the atmosphere, including cloud (Kay and Gettelman, 2009; Morrison et al., 2018), surface energy budget (Semmler et al., 2012; Boisvert et al., 2015; Boisvert and Stroeve, 2015),

precipitation (Bintanja and Selten, 2014; Kopec et al., 2016) and large-scale circulation (Chemke et al., 2019; Kennel and Yulaeva, 2020). **Figure 1** depicts the causal relations between key atmospheric variables and sea ice over the Arctic. The sea ice here represents sea ice coverage and/or sea ice thickness. Note that the processes a-d are well-known atmospheric processes, including cloud microphysics, thermodynamics, radiation, climate dynamics, which have been studied over the past few decades. The processes e-i are summarized from more recent publications, which are still under investigation by climate scientists. We will explain processes e-i in details in the next paragraph.

The arrow *e* represents the two-way effect between sea ice and net longwave flux at the surface. Based on global reanalysis (Kapsch et al., 2013; Lee et al., 2017), surface (Cox et al., 2016) and satellite observations (Huang et al., 2017), as well as model simulations (Kapsch et al., 2016; Huang et al., 2019a), the downward longwave radiation at the surface dominates surface warming and therefore enhances sea ice melt in winter and spring. The increase in downward longwave flux is a result of an increase in cloudiness and moisture in the Arctic Basin, which is caused by enhanced local evaporation or moisture transport from mid-latitudes (Luo et al., 2017). Positive anomalies of longwave flux in spring and early summer initiate an earlier melt onset, thereby triggering several feedback mechanisms which amplify melt during the succeeding months (Kapsch et al., 2016; Huang et al., 2019b). The sea ice melt increases the air temperature and thus increases the longwave flux at the



surface. The downward shortwave flux, however, appears only important after the melt has started (Kapsch et al., 2013; Huang et al., 2017). Once the surface albedo is significantly reduced due to sea ice melt, the solar radiation could be absorbed by ocean, which further accelerates ice melt in late spring and summer (Kay and Gettelman, 2009; Choi et al., 2014; Kapsch et al., 2016). The feedback between surface net shortwave flux and sea ice, represented by arrow f in Figure 1, has been confirmed by both model simulations (Kapsch et al., 2016) and satellite observations (Kay and Gettelman, 2009; Nussbaumer and Pinker, 2012; Choi et al., 2014). The arrows g indicate the interactions between the sea ice variations and atmospheric dynamical processes. A series of studies demonstrated that recent loss of Arctic sea ice is triggered by the atmospheric circulation changes such as a tendency toward a dipole pattern in the mean sea level pressure trend with an increase over the Arctic Ocean and a decrease over Siberia. The Arctic dipole anomaly in summer (Wang et al., 2009), winter (Watanabe et al.,

2006) and spring (Kapsch et al., 2019) produces a strong meridional wind (v-component) anomaly that drives more sea ice out of the Arctic Ocean. In addition, this dipole anomaly promotes transport of heat and moisture and thus enhances downward longwave radiation and control the melt onset (Huang et al., 2019b; Kapsch et al., 2019). Moreover, the changes in cyclone occurrence and/or depth during spring (Screen et al., 2011) and summer (Simmonds and Rudeva, 2012) have preconditioning effects on the sea ice cover and exert a strong influence on the amount of sea ice that survives the melt season. A recent study also pointed out that a stronger anticyclonic circulation over Greenland and the Arctic Ocean in the troposphere may have contributed as much as 60% to the September sea ice extent decline since 1979, by warming and moistening the lower atmosphere (Ding et al., 2017; Huang et al., 2021; Luo et al., 2021). On the other hand, the reduction in Arctic sea ice extent and increase in open water area in late summer are found to directly contribute to a modification of large-scale

circulation patterns in the following autumn through the additional heat stored in the Arctic Ocean and released to the atmosphere during the autumn (Overland and Wang, 2010). The increased 1,000-500 hPa thickness in autumn produce anomalous easterley zonal wind component (u-component), especially over the north of Alaska and Canada. Moreover, a more meridional flow pattern associated with sea ice reduction have an impact on the mid-latitude weather (Overland and Wang, 2010). These conclusions are mainly drawn from model simulations (Watanabe et al., 2006; Rinke et al., 2019), reanalysis and observations (Wang et al., 2009; Overland and Wang, 2010; Kapsch et al., 2019). In addition to radiation, the sensible plus latent heat flux also plays an important role in the Arctic energy budget. The increase in the downward moisture flux triggers the melting of the sea ice in spring (Boisvert et al., 2015; Boisvert and Stroeve, 2015; Marcovecchio et al., 2021). Earlier melt onset and loss of sea ice in the spring enhance warming of the ice-free ocean surface, which in turn leads to an increase of evaporation from the surface into the atmosphere in the autumn. This positive feedback between heat flux and sea ice, indicated by arrow *h*, has been confirmed by satellite observations (Boisvert et al., 2015; Boisvert and Stroeve, 2015) and model simulations (Huang et al., 2019a) during most months of the year. The arrow *i* represents the influence of precipitation on Arctic sea ice variations. Specifically, the magnitude of precipitation accumulating over the sea ice pack largely determines the depth of the snow layer, which modulates the rate of sea ice growth because of its highly insulating properties (Sturm et al., 2002). The phase of the precipitation falling on the sea ice pack is also important. As rain, it can melt, compact, and densify the snowpack, thus reducing the surface albedo and promoting sea ice melt (Perovich et al., 2002). The recent snowfall decline in summer is essentially caused by changes in precipitation form (snow turning to rain) with very little influence of decreases in total precipitation, which is a result of lower-atmospheric warming. Then the loss of snow-on-ice results in a substantial decrease in the surface albedo over the Arctic Ocean, causing additional surface ice melt by absorbing more solar radiation (Screen and Simmonds, 2012). These conclusions are mainly drawn from in-situ measurements during field campaign (Perovich et al., 2002; Sturm et al., 2002), global reanalysis products and surface observations (Screen and Simmonds, 2012; Boisvert et al., 2018; Wang et al., 2019). The higher precipitation and snowfall could result in a thicker snowpack that allows less heat loss to the atmosphere. More importantly, modeling studies suggest that increases in Arctic precipitation over the 21st century, particularly in late autumn and winter, are due mainly to strongly intensified local surface evaporation (latent heat flux) (Bintanja and Selten, 2014). Therefore, we believe that Arctic precipitation exerts direct influence on sea ice variations (arrow i), while sea ice modulates precipitation mainly through sensible plus latent heat flux (arrows h, b).

Among these studies, very few of them have demonstrated the delayed impact of one variable on another. Specifically, the net shortwave flux at the surface in early summer (May–July) is found to enhance sea ice melt with a lag of 1–4 months (Choi et al., 2014). Moreover, the sea ice condition exhibits the delayed

impacts on itself, which is called sea ice anomaly persistence (Guemas et al., 2016; Cruz-García et al., 2019; Holland et al., 2019). The sea ice anomaly persistence depends on the predictand (area, extent, volume), region, and the initial and target dates, which can be varied from a few days to a few years (Guemas et al., 2016). With sea ice anomaly persistence, there is predictability for the sea ice area in winter but low predictability throughout the rest of the year in peripheral seas. Based on multiple model simulations, the Labrador Sea stands out among the considered regions, with sea ice predictability extending up to 1.5 years (Cruz-García et al., 2019).

Note that most of studies mentioned above determine the changes in one variable, happening before another one, by applying time series analysis and/or composite analysis based on observations, reanalysis or model output (Perovich et al., 2002; Sturm et al., 2002; Kay and Gettelman, 2009; Wang et al., 2009; Nussbaumer and Pinker, 2012; Kapsch et al., 2013; Choi et al., 2014; Boisvert et al., 2015; Boisvert and Stroeve, 2015; Cox et al., 2016; Huang et al., 2017; Huang et al., 2019b; Boisvert et al., 2018; Wang et al., 2019). Among them, some studies use more advanced statistical analysis such as empirical orthogonal function (Watanabe et al., 2006; Overland and Wang, 2010) and self-organizing map (Kapsch et al., 2019; Rinke et al., 2019). Other studies assess the causal links through targeted modeling experiments (Bintanja and Selten, 2014; Kapsch et al., 2016; Ding et al., 2017; Huang et al., 2019a; Cruz-García et al., 2019), in order to test whether a manipulation of one variable has an impact on others. And most of the studies focus on relationships between only one or two atmospheric processes with changes in Arctic sea ice. Therefore, in this study, we target to provide a more comprehensive analysis about causality between multiple atmospheric processes and sea ice by applying different data-driven causality approaches.

3 DATA SETS AND DATA PRE-PROCESSING

In this study, we use the total sea ice extent as the Arctic sea ice index. The sea ice extent is defined as the total area in the Arctic with sea ice concentration greater than 15%. The conversion from sea ice concentration to sea ice extent was conducted at daily time scale. Therefore, we obtained the sea ice concentration from the Nimbus-7 SSMR and DMSP SSM/I-SSMIS passive microwave data version 1 (Cavalieri et al., 1996) provided by the National Snow and Ice Data Center. This dataset was generated from brightness temperature data, and provided daily in the polar stereographic projection with a grid box of 25 km \times 25 km since October 1978. The uncertainty of sea ice concentration over the Arctic is within $\pm 5\%$ during the winter, when the sea ice is relatively thick and the sea ice concentration is high. During the summer, the uncertainty increases to $\pm 15\%$ when the melt ponds are present (Cavalieri et al., 1992).

The atmospheric variables were obtained from ERA-5 global reanalysis product. ERA-5 was produced using 4D-Var data assimilation in CY41R2 of European Centre for Medium-Range Weather Forecasts (ECMWF)'s Integrated Forecast

TABLE 1 | The atmospheric and sea ice variables considered in this study.

Abbrev.in Figure 1	Variable					
GH	Geopotential heights averaged from 200 hPa, 500 hPa, and 850 hPa					
RH	Relative humidity averaged from 1,000-300 hPa					
SLP	Sea level pressure					
u10 m	Zonal (u-component) wind at 10 m					
v10 m	Meridional (v-component) wind at 10 m					
HFLX	Sensible plus latent heat flux					
Precip	Total precipitation					
CC	Total cloud cover					
CW	Total cloud water path					
SW	Net shortwave flux at the surface					
LW	Net longwave flux at the surface					
Sea_ice	Sea ice extent in the Northern Hemisphere					

System (IFS), with 137 hybrid sigma/pressure (model) levels in the vertical, with the top level at 0.01 hPa (Hersbach et al., 2020). The ERA-5 reanalysis has been evaluated over the Arctic in the previous studies and it stands out among several global reanalysis products (Graham et al., 2019; Mayer et al., 2019) as being more consistent with independent observations (Hersbach et al., 2020), which lends credence to the results obtained here in connection with the associations between the variables considered. In this study, the variables used in the causality discovery algorithms are listed in Table 1. For three-dimensional data (geopotential heights and relative humidity), we treat it as a single variable because we would like to filter out the connections between different layers for each variable. The air temperature has been excluded in this study because it exhibits very high correlation with sea ice concentration. The interactions between air temperature and sea ice could be dominant over all other atmospheric processes based on our tests.

All monthly gridded data during 1980-2018 have been averaged over the Arctic north of 60°N (Figure 2) using areaweighted method. Therefore, we created the time-series for both sea ice extent and atmospheric variables. We believe that 39 years of data should be sufficient to derive causal relationships and draw meaningful conclusions. In addition, most of the observational-based climate studies mentioned in Figure 1 used the data during the modern satellite era (1979-present), which is consistent with our studies. Our purpose is to match this time period and to determine whether those algorithms can produce similar results. Under the background of global warming, almost all components in the Earth System changed with time, as a response to increased greenhouse gas emissions. Regressing atmospheric responses against sea ice decline (or the other way around) involves the risk of finding potentially spurious atmosphere-sea ice interactions simply because both variables change across years (Iler et al., 2017). Therefore, it is necessary to detrend the time-series as the climate data is normally nonlinear and nonstationary (Wu et al., 2007). This technique has been widely used in previous climate studies (Weber and Talkner, 2001; Kawale et al., 2013), including several recent studies about atmosphere-sea ice interactions in the Arctic (Ding et al., 2017; Huang et al., 2017; Baxter et al., 2019; Topál et al., 2020). Moreover, detrending for time-series that is nonstationary is also important in causality discovery methods (Granger, 1969; Entner and Hoyer, 2010; Peters et al., 2012; Runge et al., 2019). Thus, in order to eliminate overall impacts of global warming and seasonality during this 39-year time period, we applied detrending and deseasonalizing for each time-series. Note that we also conducted additional analysis with raw data to show how detrending and deseasonalizing have an impact on our results at the end of **Section 5**.

Here we assume the time series is additive and there exist both trend and seasonal components, that is

$$X_t = m_t + s_t + Y_t. (1)$$

Here, the m_t indicates the trend component, while the s_t represents seasonality component. The time series has been detrended by subtracting the line of best fit from the time-series m_b where the line of best fit was obtained from a linear regression model with the time steps as the predictor. To deseasonalize the time-series, we used averaged seasonal index s_t to seasonally adjust the data. The seasonal index were calculated from moving averages with a 12-months seasonal window in this study (Hamilton, 1994). More details about time series decomposition can be found in Brockwell et al. (2016). At the end, we only kept the residual component Y_b which fluctuates around zero, that is

$$E(Y_t) = 0. (2)$$

Then we normalized Y_t using the max-min method so that

$$Y_t \in [0,1]. \tag{3}$$

4 DATA-DRIVEN CAUSALITY DISCOVERY ALGORITHMS

In this work, we apply data-driven causal discovery algorithms aiming to find the major causes of the decrease of Arctic sea ice. These algorithms typically assume one process or state, a cause, contributes to the production of another process or state, an effect. The cause is assumed to be partly responsible for the effect, and the effect is partly dependent on the cause. Although it is not necessary that the effect will have a reverse *affect* on the cause. Thus, causal discovery aims to discover direct cause-effect relationships for both instantaneous and delayed causes. Here we will investigate three recently proposed causal discovery algorithms: TCDF (Nauta et al., 2019), NOTEARS (Zheng et al., 2018), and DAG-GNN (Yu et al., 2019). The overall framework of our benchmarking pipeline is shown in **Figure 3**. We believe this general framework can help researchers to evaluate their causality discovery approaches in sea ice study and Earth science in general.

4.1 Temporal Causality Discovery Framework

The TCDF algorithm (Nauta et al., 2019) is based on attention-based (Yin et al., 2016) Convolutional Neural Networks (CNN). The input to the algorithm is time series data and the output is a causality graph structure with time delay or lag, which is automatically determined by

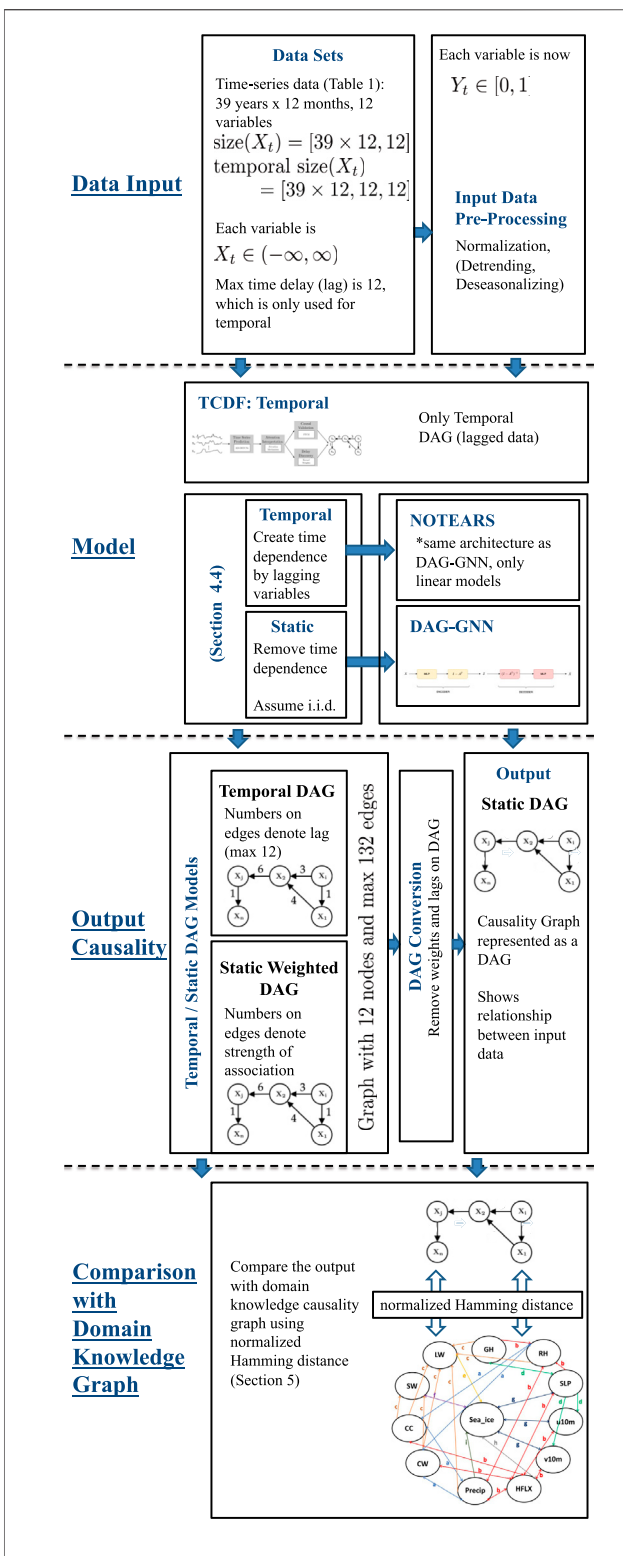
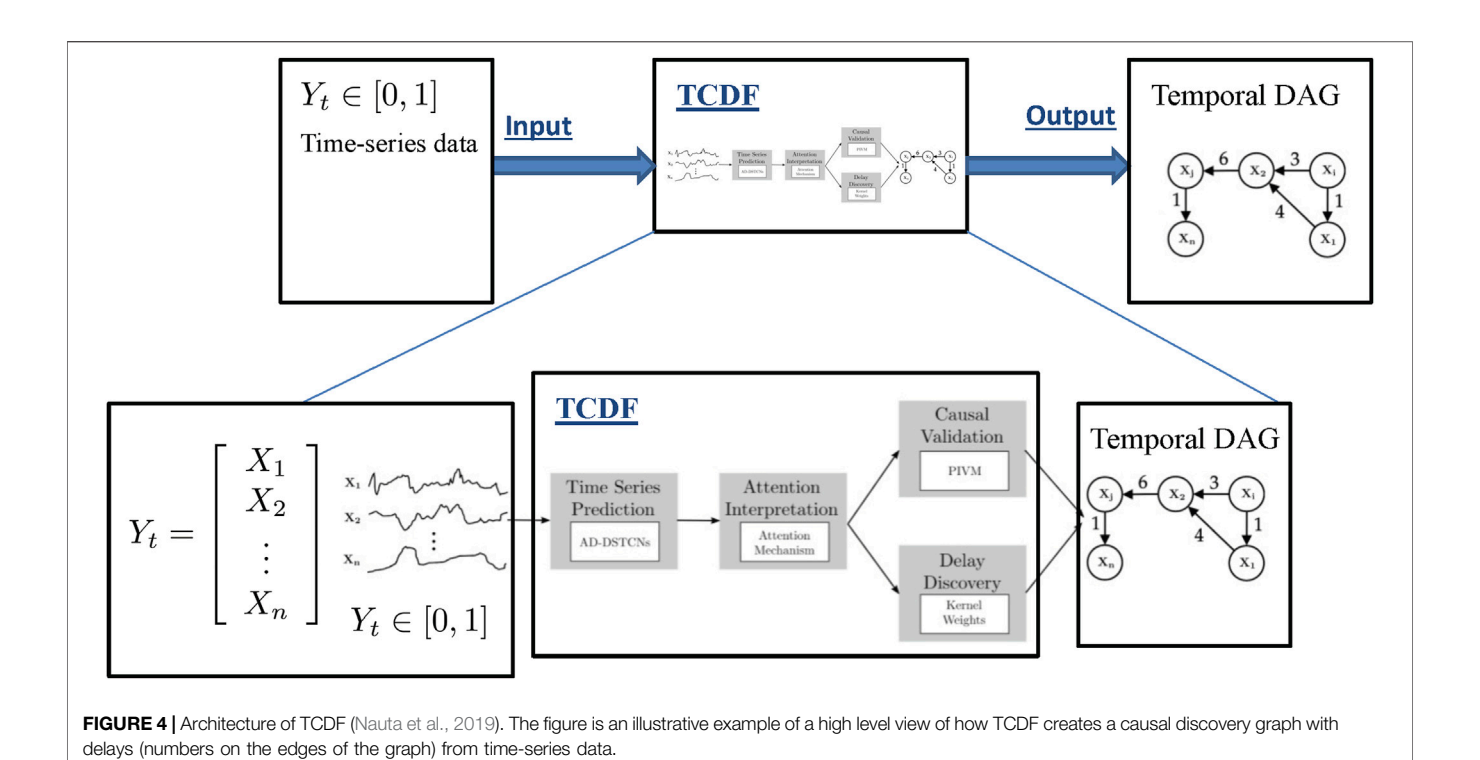


FIGURE 3 | The framework of benchmarking causality discovery methods in atmosphere-sea ice study. Note that detrending and deseasonalizing time-series is optional during the input data pre-processing process.

the TCDF algorithm. For our climate sciences problem with data shown in Table 1, the TCDF algorithm takes the measured data of sea ice, relative humidity, and other atmospheric processes (Table 1) in order to build a causality graph for the input data interact with each other. Figure 4 illustrates the architecture of the TCDF method, operating on generic data, where the multi-dimensional time-series data is on the left and the produced causality graph is on the right. There are four steps to learn a Temporal Causal Graph from the timeseries data: Time Series Prediction block, Attention Interpretation block, Causal Validation and Delay Discovery blocks as explained in detail in Nauta et al. (2019). Here we explain the general process of the TCDF algorithm where a more in depth description is in section 4 of Nauta et al. (2019). The first step is that the time-series data is fed into the Time Series Prediction block, which tries to create an internal time-series model that will accurately try to model each atmospheric or atmosphere-sea ice process. Then the Attention Interpretation block takes that hidden model produced by the Time Series Prediction block and tries to verify and validate how accurate the prediction is to the actual data. Then the last two blocks again verify the hidden model from the Time Series Prediction block but now using the verification errors from the Attention Interpretation block in parallel. The two last blocks try to verify the causal and time delay relationships generated from the prediction block with errors generated by the attention block. A detailed explanation is provided in Nauta et al. (2019) and more details on attentionbased CNN can be found in Yin et al. (2016). Also as a side note: for multi-dimensional time-series there are *n* independent attentionbased CNNs, all with the same architecture for each time-series data.

The basic structure of TCDF is for time-series prediction as seen in the first step of the framework in Figure 4. After predicting time-series, the output gives attention scores for the attention interpretation mechanism. Attention CNNs (Yin et al., 2016) is a machine learning method based on using neural networks to help optimize internal automatically picked parameters in the hidden model generated in our case from the Time Series block. In other words, it is a form of self-learning or adaptive optimization (Eveleigh, 1967; Wei, 2018) applied to machine learning. The causality validation reads the final result of the attention scores and applies a permutation importance validation method. The permutation importance is a measurement of how much an error will affect the values of a certain attention score when all scores are randomly permuted. The idea is that permuting a time-series attention score removes potential cause and effect relationships and hence the method can detect real versus fake causal relationships. In parallel the attention scores are fed to the delay discovery to learn the potential delay in cause and effect relationships. The delay discovery also employs the permutation importance validation method.

Another major advantage of TCDF is in using a CNN versus a traditional Recurrent Neural Network (RNN), such as a Long Short Term Memory (LSTM), for time-series data. The advantage is that RNNs typically have a vanishing gradient problem: long-term information has to sequentially travel through all the cells before getting to the present processing cell and typically stalls the learning processes, sometimes even preventing any further



improvements gained with learning with more data (Hochreiter, 1998; Tan and Lim, 2019). This is greatly amplified when the number of layers becomes very deep, typically more than 10 layers (Schmidhuber, 2015). Though a CNN structure might have this problem as well, it is more common in RNN because it typically needs much more memory and cells than a CNN structure. With more cells to process, there is a greater chance of obtaining the vanishing gradient problem.

4.2 Non-combinatorial Optimization *via* Trace Exponential and Augmented lagrangian for Structure learning

The NOTEARS algorithm (Zheng et al., 2018) assumes a linear data generating model of the form

$$X_{i} = \sum_{j: W_{ji} \neq 0} W_{ji} X_{j} + N_{i}, \tag{4}$$

where W is the weighted adjacency matrix of the underlying causality graph G(W), that is $j \to i$ in G(W) if and only if $W_{ji} \neq 0$, and the random variables N_i are independent noise variables. Given n independent and identically distributed (i.i.d.) observations of the variables X_1, \ldots, X_d , written as matrix $\mathbf{X} \in {}^{n \times d}$, a standard estimator for W is the (regularized) least-squares estimator

$$\widehat{W} = \underset{W \in d^{\times d}}{\operatorname{arg}} \frac{1}{2n} \|\mathbf{X} - \mathbf{X}W\|_F^2 + \lambda \|W\|_1 \quad \text{subject to } G(W) \text{ is a DAG,}$$
(5)

where $\lambda \geq 0$ is the regularization parameter. This estimator is theoretically well-studied and satisfies desirable properties such

as consistency (Van de Geer and Bühlmann, 2013; Loh and Bühlmann, 2014; Aragam et al., 2017). However, due to the non-convex, *combinatorial-like* constraint, optimization problems of the form **Eq. 5** are NP-hard to solve (Chickering, 1996), and hence unless the number of variables *d* is very small, heuristics such as local search have to be applied (e.g., Heckerman et al., 1995; Ramsey et al., 2017). The NOTEARS algorithm builds on the insight that

$$G(W)$$
 is a DAG \Leftrightarrow trace $(\exp(W \circ W)) - d = 0$, (6)

where exp denotes the matrix exponential and ° the element-wise product. The characterization (6) allows to treat the optimization problem Eq. 5 as an ordinary *continuous* constrained optimization problem and to use any algorithm from the rich literature on continuous optimization to find a locally optimal solution to (5). Concretely, the NOTEARS algorithm applies the augmented Lagrangian method (e.g., Nocedal and Wright, 2006) to search for a locally optimal solution to

$$\arg\min_{W\in^{d\times d}}\frac{1}{2n}\|\mathbf{X}-\mathbf{X}W\|_F^2+\lambda\|W\|_1\quad\text{subject to trace }(\exp\left(W\circ W\right))-d=0.$$

After applying the augmented Lagrangian method to (7) and obtaining an output W, the final step of the NOTEARS algorithm is to "round" \tilde{W} and to set all entries of \tilde{W} with absolute value smaller than some threshold t to zero. This yields the final output \hat{W} of the NOTEARS algorithm.

In summary, the NOTEARS algorithm yields an estimate of the underlying causality graph as well as the strengths of the causal relationships. It does so by assuming a linear data generating model and access to i.i.d. observations and fitting a

causal graph to the data. Its advantage over existing approaches is that it formulates the fitting problem in a way that makes it amenable to standard algorithms for continuous optimization. However, in general, the NOTEARS algorithm will still return only a locally optimal solution to the fitting problem, and the assumption of a linear data generating model might restricts its applicability.

4.3 Directed Acyclic Graph-Graph Neural Networks

DAG-GNN (Yu et al., 2019) can be thought of as an extension to the NOTEARS algorithm (Zheng et al., 2018) in that the proposed method assumes a nonlinear model of the form

$$X = f_2((I - A^T)^{-1} f_1(Z)), \tag{8}$$

where Z is the encoded latent variable of X. This can be contrasted to the linear model assumed in NOTEARS

$$X = (I - A^{T})^{-1}Z, (9)$$

where **Eq. 9** is a restructured form of **Eq. 4**. Further, DAG-GNN builds an inference model to encode *Z*, given by

$$Z = f_4((I - A^T)f_3(X)), (10)$$

where f_3 and f_4 play a conceptually inverse role for f_2 and f_1 respectively. In particular, this paper assumes f_1 , f_4 to be identity functions and f_2 , f_3 as Multilayer Perceptrons (MLP). Multilayer Perceptrons are feed-forward Artificial Neural Networks with multiple hidden layers. They are trained through stochastic gradient descent and backpropagation and their function (f_2 and f_3 in our case) corresponds to the relation between the input and output variables.

Since an MLP is nonlinear, it should in theory capture any nonlinearities in the data better than NOTEARS which is a linear model. This is further explained in **Figure 5** where *X* is the regenerated form of *X* and MLP has one hidden layer of 64 neurons. Further, DAG-GNN minimizes the following loss function.

$$\min_{A,\theta} f(A,\theta) = -L_{ELBO} \tag{11}$$

s.t.
$$h(A) = \text{tr}[(I + \alpha A \circ A)^m] - m = 0,$$
 (12)

where the unknowns include the weight matrix A, and parameters θ for Variational Autoencoder (VAE). Further, ELBO is the Evidence Lower Bound of the VAE adopted from (Kingma and Welling, 2014) and h(A) is used to solve the augmented Lagrangian as done in (Nocedal and Wright, 2006).

So DAG-GNN is a more robust, non-linear model which can learn more complex relationships than NOTEARS. Having an MLP as a backbone it is capable of learning from a large training set, and giving accurate results. Furthermore, autoencoders have been proven to be useful for unsupervised learning and feature extraction. This makes DAG-GNN capable for understanding causal relationships between atmospheric variables.

4.4 Static Versus Temporal Model

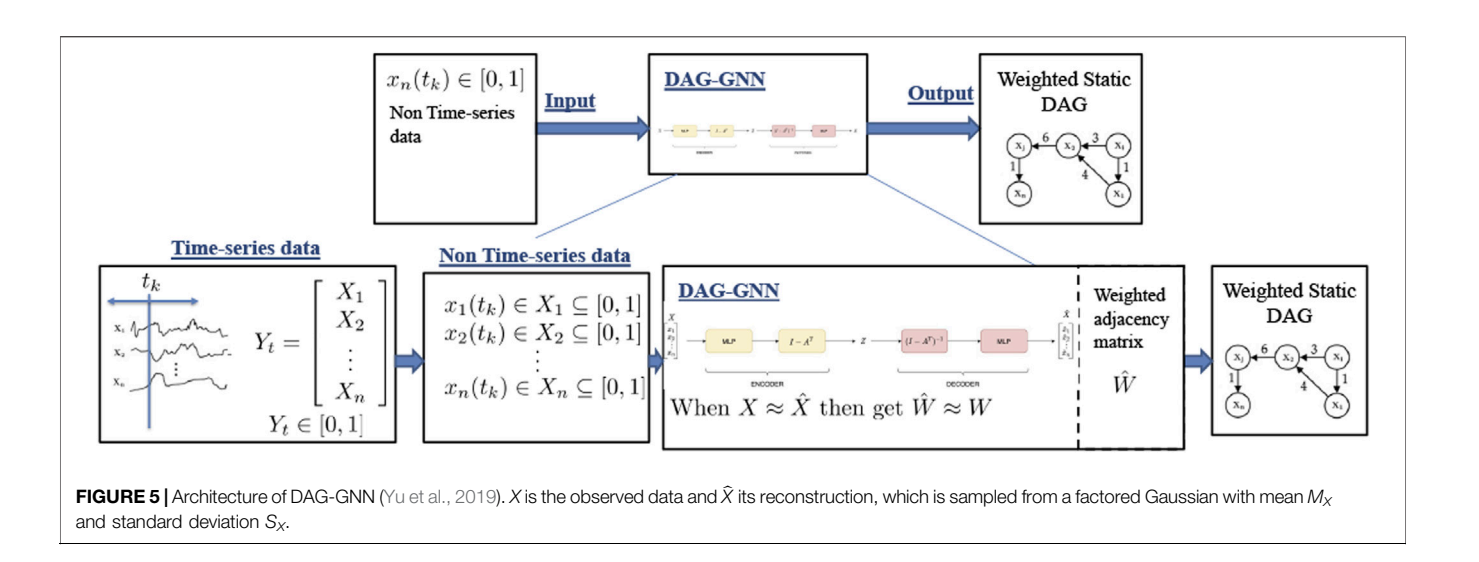
While TCDF requires time series data as input and explicitly models time delay of causal relations, NOTEARS and DAG-GNN assume to

be provided i.i.d. observations of the variables. Similarly to other causal discovery studies in climate research (Ebert-Uphoff and Deng, 2012), we apply the latter two methods in two ways: in the static model, we treat the observations of the variables summarized in **Table 1** at different points in time as i.i.d. observations and directly feed the data into the two methods. Alternatively, in the temporal model, we first augment the data set by adding lagged versions of each variable, that is for each variable X we additionally consider variables X^1, X^2, \ldots, X^{12} , where X^k is a version of the variable X that is measured with a lag of k time units (in our case: months) compared to X. Here, the maximum time lag we consider is 12 months since we want to focus on causal links from sub-seasonal to seasonal timescales. We then treat the observations of the various variables at different points in time as i.i.d. observations and run NOTEARS and DAG-GNN, respectively. The graphs produced by these methods, using the augmented data, are assumed to encode the time delay of causal relations. However, in order to obtain a causal graph on the variables of Table 1 we generate a "reduced" temporal graph from these "full" temporal graphs by connecting two variables *X* and *Y* in the reduced temporal graph whenever any of the variables X, X^1, \ldots, X^{12} is connected to any of Y, Y^1, \ldots, Y^{12} in the full temporal graph. The reduced temporal graph is the output of the temporal model.

5 RESULTS

In this section we present some results of the three causal discovery algorithms introduced in **Section 4**. We study how the causality graphs produced by the three methods depend on the choice of hyperparameters and see that the graphs can be quite different for varying hyperparameters. We work with the normalized Hamming distance (ignoring the edge weights in the graphs produced by NOTEARS or DAG-GNN) and also compare all graphs to the domain knowledge graph (**Figure 1**). Note that We do not quantify the strength of causal relationships in the domain knowledge graph, and we evaluate the algorithms in terms of whether they are capable of detecting these causal relationships, but not in terms of estimating the strength of relationships.

In this section, we treat all graphs as unweighted graphs. The normalized Hamming distance is a widely used metric to compare two unweighted graphs on the same set of vertices (Donnat and Holmes, 2018). Let A, $B \in \{0,1\}^{m \times m}$ be the adjacency matrices of two unweighted graphs G_A , G_B on m vertices. The normalized Hamming distance between G_A and G_B is given by $dist_{HD}(G_A, G_B) = \frac{1}{m^2} \sum_{i,j=1}^m 1\{A_{ij} \neq B_{ij}\}$, that is the number of edges that are present in one graph but not in the other, normalized by the number of all possible edges. The normalized Hamming distance between G_A and G_B is zero if and only if G_A and G_B coincide, and it is at most one (which happens if one graph is empty, i.e., does not have any edges, and one graph is complete, i.e., any two vertices are connected). In the following, for each of the three causal discovery algorithms introduced in Section 4 we compute the normalized Hamming distance between the graphs produced by an algorithm for different values of its hyperparameters. We also compare the graphs to the domain knowledge graph shown in Figure 1 which is generated based on current literature.



5.1 Causality Discovery Results Based on Temporal Causality Discovery Framework Approach

Table 2 shows the values for the normalized Hamming distance for the TCDF method, which quantifies the similarity of two causality graphs. A smaller number indicates that two causality graphs are more similar to each other. Two hyperparameters that were chosen are the kernel size, which is how many data points are combined together, and the number of hidden layers, which perform nonlinear transformations of the inputs entered into the network. The number of hidden layers corresponds to the number of hidden CNN layers in the TCDF algorithm. It seems that the addition of a hidden layer leads to far worse results and even produces no causality graphs as is the case for when kernel = 4 and kernel = 6 for layer = 1. The kernel size is related to how much the TCDF method lags the variables for the causality study. The default setting for the hyperparameters as shown with ♣ in Table 2 produce TCDF's best result when comparing to the domain knowledge graph, but that is nowhere close to the domain knowledge graph shown in Figure 1. It seems that the TCDF method does not produce good results for our Arctic Sea Ice data.

5.1.1 Comparison Between Temporal Causality Discovery Framework Based Causality Graph and Domain Knowledge Graph

Since the TCDF focuses on time series, only the temporal graph that is closest to the domain knowledge graph is shown (**Figure 6**). In general, if the causality graph generated by the algorithm looks similar to **Figure 1**, we believe that this approach is more capable of capturing the real causal relationships in the Arctic. There is no cause and effect between sea ice and any atmospheric variables. As for the causality within the atmosphere, only a few edges (cause-effect relationships) are generated by the TCDF algorithm. Among them, the feedback between u10 m and v10 m, as well as the impact of SW on CW are not consistent with domain knowledge.

5.2 Causality Discovery Results Based on Non-combinatorial Optimization *via* Trace Exponential and Augmented lagrangian for Structure learning Approach

The NOTEARS algorithm has two hyperparameters $\lambda \geq 0$ and $t \geq 0$ as explained in **Section 4.2**: the parameter λ is the regularization parameter (cf. **Eq. 5**) and t is the threshold for setting edge weights of the preliminary output to zero (cf. end of **Section 4.2**). There is no default value for λ , but in the main experiment that comes with the NOTEARS code (Zheng et al., 2018), the authors use $\lambda = 0.1$ and hence we consider that value to be the default value. Furthermore, we observed that choosing a value larger than 0.1 for λ often results in an empty graph as the output of NOTEARS. The default value for t is t=0.3. Indeed, we observed that t=0.3 yields better results when comparing to the domain knowledge graph than other values of t.

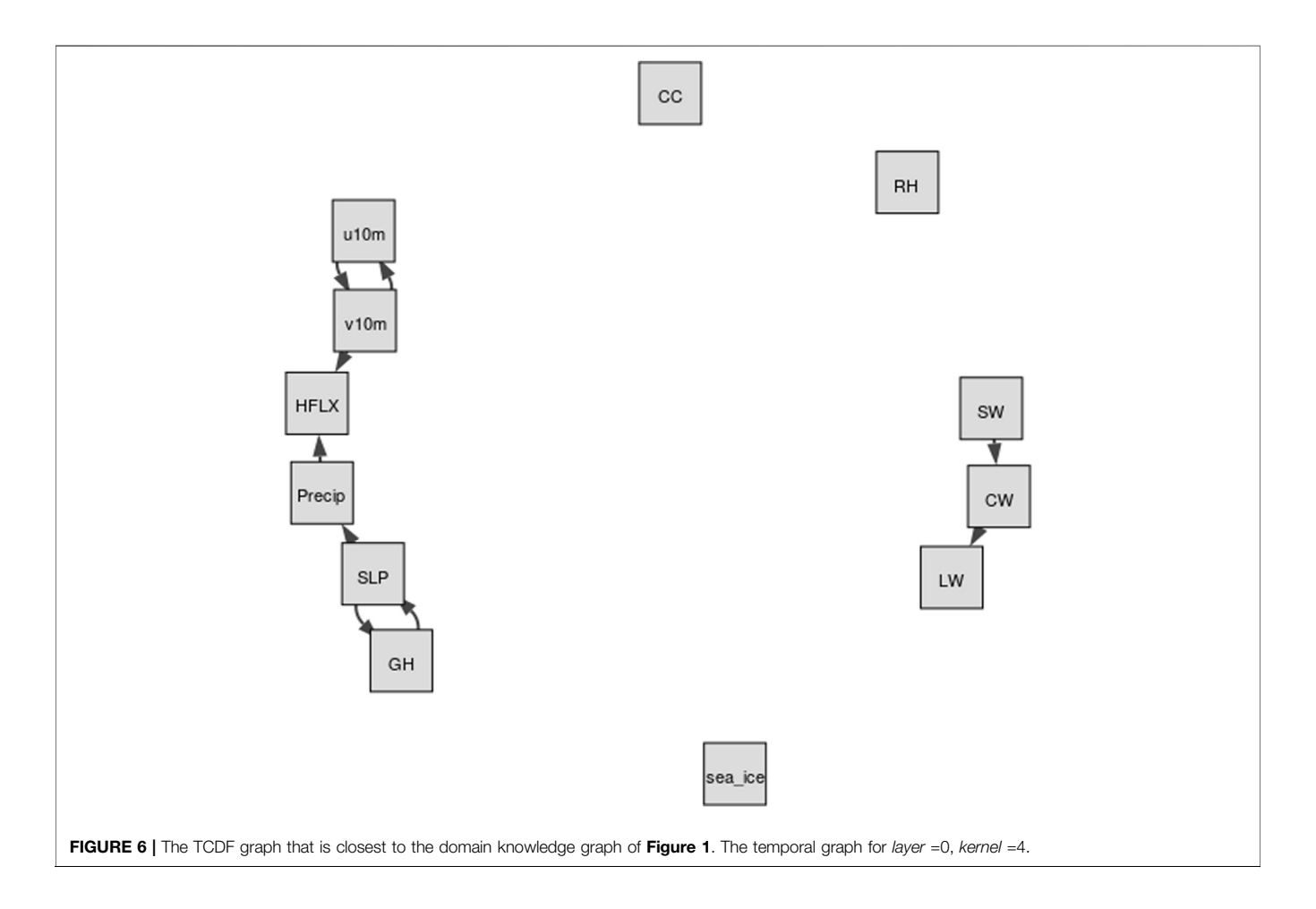
Table 3 shows the normalized Hamming distance between the graphs produced by NOTEARS for $\lambda \in \{0, 0.1\}$ and $t \in \{0.2, 0.3\}$, for both the static and the temporal model. The last row of the table shows the normalized Hamming distance between the various graphs and the domain knowledge graph of **Figure 1**. Note that actually none of the graphs considered here is a DAG. We can see that the distances between the various temporal graphs (middle right part of the table) are significantly larger than the distances between the various static graphs (upper left part of the table). We can also see that changing the value of λ from 0 to 0.1 causes a larger difference in the result than changing the value of t from 0.2 to 0.3 (e.g., the normalized Hamming distance between the static model with $\lambda = 0$, t = 0.2 and the static model with $\lambda = 0$, t = 0.3 is only 0.02, while the distance between the static model with $\lambda = 0$, t = 0.2 and the static model with $\lambda = 0$. 1, t = 0.2 is 0.15).

5.2.1 Comparison Between Non-combinatorial Optimization *via* Trace Exponential and Augmented lagrangian for Structure learning Based Causality Graph and Domain Knowledge Graph

In **Figure 7**, we show both the static and the temporal graphs that are closest to the domain knowledge graph of **Figure 1**. The larger weights

TABLE 2 Distance matrix with respect to the normalized Hamming distance for TCDF. ♣ denotes *layer* =0, *kernel* =4 are the algorithm's default hyperparameters. The bottom row compares to the domain knowledge graph of **Figure 1**, with the best values being marked in bold.

		Temporal						
		layer = 0	layer = 0	layer = 0	layer = 1	layer = 1	layer = 1	
		kernel = 2	kernel = 4 ⁺	kernel = 6	kernel = 2	kernel = 4	kernel = 6	
Temporal	layer = 0, kernel = 2	0	0.05	0.01	0.02	0.01	0.01	
	layer = 0, kernel = 4♣	0.05	0	0.06	0.07	0.06	0.06	
	layer = 0, $kernel = 6$	0.01	0.06	0	0.01	0.01	0.01	
	layer = 1, kernel = 2	0.02	0.07	0.01	0	0.02	0.02	
	layer = 1, kernel = 4	0.01	0.06	0.01	0.02	0	0	
	layer = 1, kernel = 6	0.01	0.06	0.01	0.02	0	0	
	Domain knowl	0.35	0.33	0.34	0.34	0.33	0.33	



in the causality graph indicate a stronger relationship between two variables. Generally, while none of the produced graphs is really close to the domain knowledge graph, the static graph looks more reasonable.

In the static graph, the RH and precipitation seem to dominate the sea ice changes, with weights of 0.55 and 0.41, respectively. In the meantime, the sea ice exerts large influence on SW (weight of 0.79) and CW (weight of 0.31). The causal relations between precipitation, SW and sea ice in the domain knowledge graph of **Figure 1** are well captured by the NOTEARS algorithm. However, RH and CW are believed to be only indirectly connected with sea ice changes (i.e., in

the domain knowledge graph there is no direct connection between RH or CW and sea ice), but in the static graph produced by the NOTEARS algorithm there are direct connections. The causality between each two atmospheric variables is generally reasonable based on the domain knowledge graph. The connections between CW and v10 m, SW and v10 m, and v10 m and u10 m are not quite consistent with the domain knowledge graph. However, those connections may be physically reasonable because winds are related to changing temperatures, humidity, clouds and radiation through advection in a broader area. Compared with the static graph,

TABLE 3 Distance matrix with respect to the normalized Hamming distance for NOTEARS. \bullet denotes that $\lambda = 0.1$, $t = 0.3$ are the algorithm's default hyperparameters. The
bottom row compares to the domain knowledge graph of Figure 1, with the best values being marked in bold.

		Static				Temporal				
		$\frac{\lambda=0}{t=0.2}$		$\frac{\lambda = 0.1}{t = 0.2}$	$\frac{\lambda = 0.1}{t = 0.3^{+}}$	$\frac{\lambda=0}{t=0.2}$	$\frac{\lambda=0}{t=0.3}$	$\frac{\lambda = 0.1}{t = 0.2}$	$\frac{\lambda = 0.1}{t = 0.3^{4}}$	
Static	$\lambda = 0, t = 0.2$	0.0	0.02	0.15	0.15	0.54	0.36	0.16	0.15	
	$\lambda = 0, t = 0.3$	0.02	0.0	0.15	0.12	0.53	0.35	0.14	0.12	
	$\lambda = 0.1, t = 0.2$	0.15	0.15	0.0	0.02	0.51	0.36	0.09	0.1	
	$\lambda = 0.1, t = 0.3^{-4}$	0.15	0.12	0.02	0.0	0.52	0.35	0.07	0.08	
Temporal	$\lambda = 0, t = 0.2$	0.54	0.53	0.51	0.52	0.0	0.18	0.48	0.51	
	$\lambda = 0, t = 0.3$	0.36	0.35	0.36	0.35	0.18	0.0	0.33	0.34	
	$\lambda = 0.1, t = 0.2$	0.16	0.14	0.09	0.07	0.48	0.33	0.0	0.03	
	$\lambda = 0.1, t = 0.3^{-4}$	0.15	0.12	0.1	0.08	0.51	0.34	0.03	0.0	
	Domain knowl.	0.35	0.33	0.36	0.35	0.54	0.46	0.37	0.35	

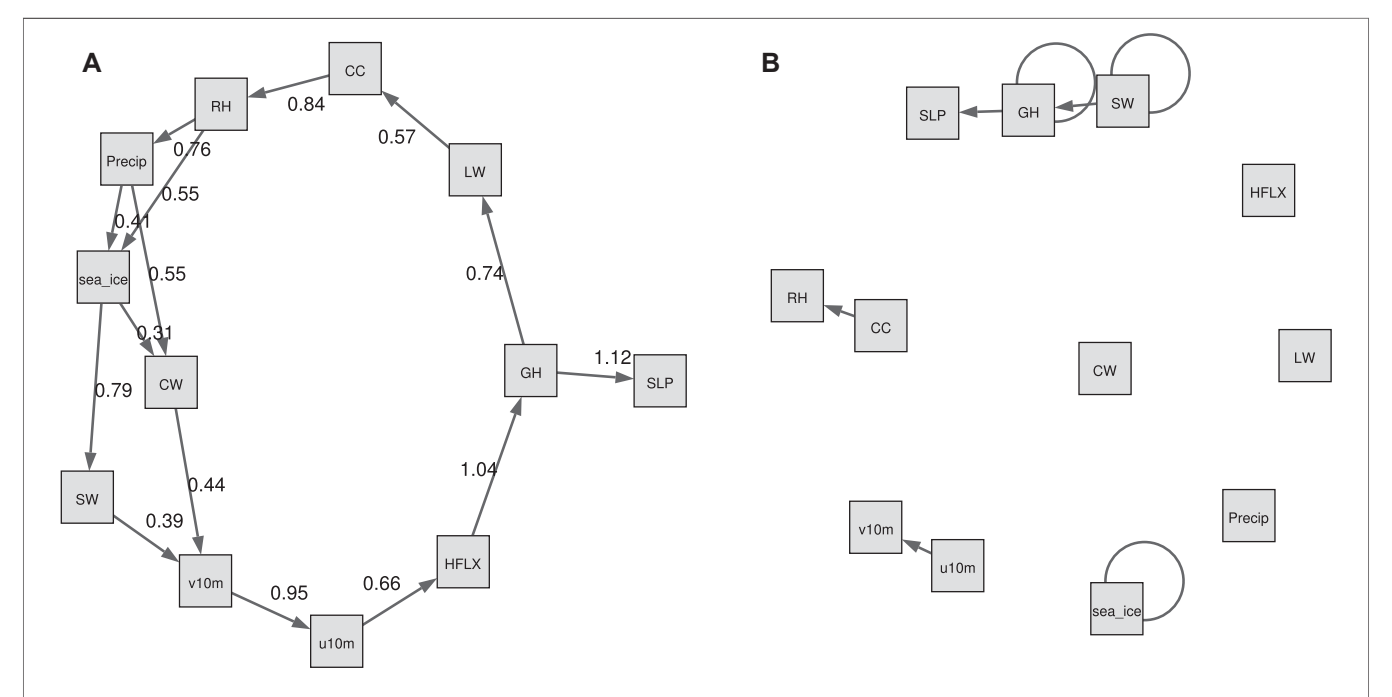


FIGURE 7 | The NOTEARS graphs that are closest to the domain knowledge graph of **Figure 1**, with respect to the normalized Hamming distance as shown in **Table 3**. (**A**): The static graph for $\lambda = 0$, t = 0.3. Note that in **Table 3** this graph is treated as an unweighted graph. The edge weights are estimates of the coefficients W_{jj} in the data generating model (4). The larger weights indicate stronger connection between two variables. (**B**): The temporal graph for $\lambda = 0.1$, t = 0.3.

the temporal graph detects only very few edges. It shows that the sea ice, SW and GH have delayed impacts on themselves, demonstrating both sea ice and atmosphere have a degree of seasonal to year long climate predictability. Note that the NOTEARS does not model time delay of causal relations as mentioned in **Section 4.4** and the temporal graphs that we produced using this algorithm do not contain straightforward-to-interpret time lag information.

5.3 Causality Discovery Results Based on Directed Acyclic Graph-Graph Neural Networks Approach

Like the NOTEARS algorithm, DAG-GNN has two hyperparameters: $\tau \ge 0$ and $t \ge 0$, where τ is similar to λ used

in NOTEARS. We noticed that the hyperparameter τ is very sensitive, and show the outputs for only two values of τ i.e., $\tau \in \{0, e-7\}$. We vary t similar to NOTEARS, and test for $t \in \{0.2, 0.3\}$. **Table 4** tabulates the normalized Hamming Distance computed between all the graphs obtained by varying these two hyperparameters. Further, we computed the Normalized Hamming Distance between all these graphs and the domain knowledge graph of **Figure 1**. In order to carry out this specific computation, we created unweighted matrices from the weighted outputs of DAG-GNN with the help of absolute thresholding using the hyperparameter t.

From **Table 4**, we see that the least normalized Hamming Distance with the Domain Knowledge Graph is obtained by $\tau = e - 7$, t = 0.3 for the static model and $\tau \in \{0, e - 7\}$, t = 0.3 for the

TABLE 4 Distance matrix with respect to the normalized Hamming distance for DAG-GNN. ♣ denotes the algorithm's default hyperparameters. The bottom row compares to the domain knowledge graph of **Figure 1**, with the best values being marked in bold.

		Static			Temporal				
		$\frac{\tau=0}{t=0.2}$	$\frac{\tau = e - 7}{t = 0.3^{4}}$	$\frac{\tau=0}{t=0.2}$	$\frac{\tau = e - 7}{t = 0.3}$	t = 0.2	t = 0.3*	<i>t</i> = 0.2	t = 0.3
Static	$\tau = 0, t = 0.2$	0.0	0.06	0.04	0.07	0.1	0.12	0.1	0.12
	$\tau = 0, t = 0.3^{-4}$	0.06	0.0	0.05	0.01	0.08	0.07	0.08	0.07
	$\tau = e - 7$, $t = 0.2$	0.04	0.05	0.0	0.06	0.08	0.1	0.08	0.1
	$\tau = e - 7$, $t = 0.3$	0.07	0.01	0.06	0.0	0.08	0.08	0.08	0.08
Temporal	$\tau = 0, t = 0.2$	0.1	0.08	0.08	0.08	0.0	0.03	0.01	0.03
	$\tau = 0, t = 0.3^{-4}$	0.12	0.07	0.1	0.08	0.03	0.0	0.05	0.0
	$\tau = e - 7$, $t = 0.2$	0.1	0.08	0.08	0.08	0.01	0.05	0.0	0.05
	$\tau = e - 7$, $t = 0.3$	0.12	0.07	0.1	0.08	0.03	0.0	0.05	0.0
	Domain knowl	0.33	0.33	0.35	0.32	0.35	0.34	0.36	0.34

temporal model. Both the temporal models of t=0.3 give the same graphs, which is shown in **Figure 8** on the right. For the static model however, these optimum values of τ and t produce a graph which shows no relation between sea ice and other atmospheric variables. Hence, we reject it. The second most optimum graph showing a dependence of sea ice with atmospheric variables is shown in **Figure 8** on the left. Its hyperparameters are $\tau=0$ and t=0.2. Further, we note that for the temporal model, the best graphs are obtained with t=0.3, which is one of the default parameters used and suggested by the authors in (Yu et al., 2019).

5.3.1 Comparison Between Directed Acyclic Graph-Graph Neural Networks Based Causality Graph and Domain Knowledge Graph

The static and the temporal graphs closest with the domain knowledge graph are shown in Figure 8. Compared to NOTEARS, both static and temporal graphs produced by DAG-GNN are more complicated. The dynamical fields (u10 m and v10 m) dominate the sea ice changes, but with relatively small weights 0.21 and -0.25, respectively. Here, the positive (negative) edge weights indicate a positive (negative) causal effect. In this case, the negative weights between v10 m and sea ice suggest that increasing v10 m tends to decrease sea ice. Stronger northward winds can enhance ice melt by increasing ice drifting (Spreen et al., 2011) and bringing more heat and moisture from lower latitudes (Zhang et al., 2013). In the meantime, positive zonal winds (u10 m) generally isolate the Arctic from mid-latitudes, leading to cooling (in winter) and thus more sea ice (Overland and Wang, 2010). As for the causal relations between multiple atmospheric processes, they are generally reasonable compared to Figure 1. Similar as NOTEARS, the connections between u10 m and v10 m (0.95), SW and v10 m (0.25), CW and v10 m (0.32) are not reasonable and consistent with domain knowledge graph. As mentioned earlier, this is most likely because we averaged these variables in the Arctic region and those variables may exhibit relatively high correlations over a large domain. Note that the increased CW and CC tend to reflect solar radiation back to the space, leaving less SW reaching at the surface. This negative relationships between CC, CW, and SW are captured by the DAG-GNN, however, the direction of arrows are

not meaningful. The same issue occurs in the temporal graph. In addition, the sea ice has the delayed impacts on itself, but with no connection with any atmospheric processes in temporal graph. Like static graph, the causality between u10 m and v10 m as well as CW and v10 m is not consistent with domain knowledge graph. Similar as NOTEARS, DAG-GNN does not model time delay of causal relations as well.

5.4 Sensitivity Tests

We conducted additional tests with slightly different datasets to show how the causality discovery approaches are sensitive to the data. Because the results above are based on the detrended and deseasonalized data sets, the first sensitivity test we did is with raw data. Here, we show the similar static graphs as Figures 7, 8, but with raw data in Figure 9. The TCDF still does not generate meaningful edges between atmospheric components and sea ice (not shown). The NOTEARS produces different results between raw data and detrended data. Using raw data, CC, GH, LW and SW dominate sea ice changes. In comparison, RH and precipitation have a large influence on sea ice variations based on detrended and deseasonalized data. The DAG-GNN also generates more complicated results with raw data. In particular, CW, GH, SLP, LW, and SW are found to dominate sea ice variations, which show similar results as NOTEARS. Note that both NOTEARS and DAG-GNN cannot capture the response in atmosphere to sea ice variations using raw data. As mentioned earlier, the relationships obtained from detrended and deseasonalized data represent natural variability, while raw data provides information about actual changes.

The second sensitivity test we carried out is with dataset that also includes air temperature (averaged from 1,000–300 hPa). In **Figure 10**, we show the similar static graphs as **Figures 7**, **8**, but include variable "Temp". In general, the TCDF does not generate any meaningful results (not shown). The NOTEARS shows that temperatures have a large impact on the LW and HFLX, which is physically meaningful based on Stefan-Boltzmann law. In this case, RH dominates the changes in sea ice, while sea ice exerts large influence on SW. These results are similar to **Figure 7**, in which we excluded temperature. According to results produced by DAG-GNN, temperatures have an impact on SLP, HFLX, CC, RH, LW,

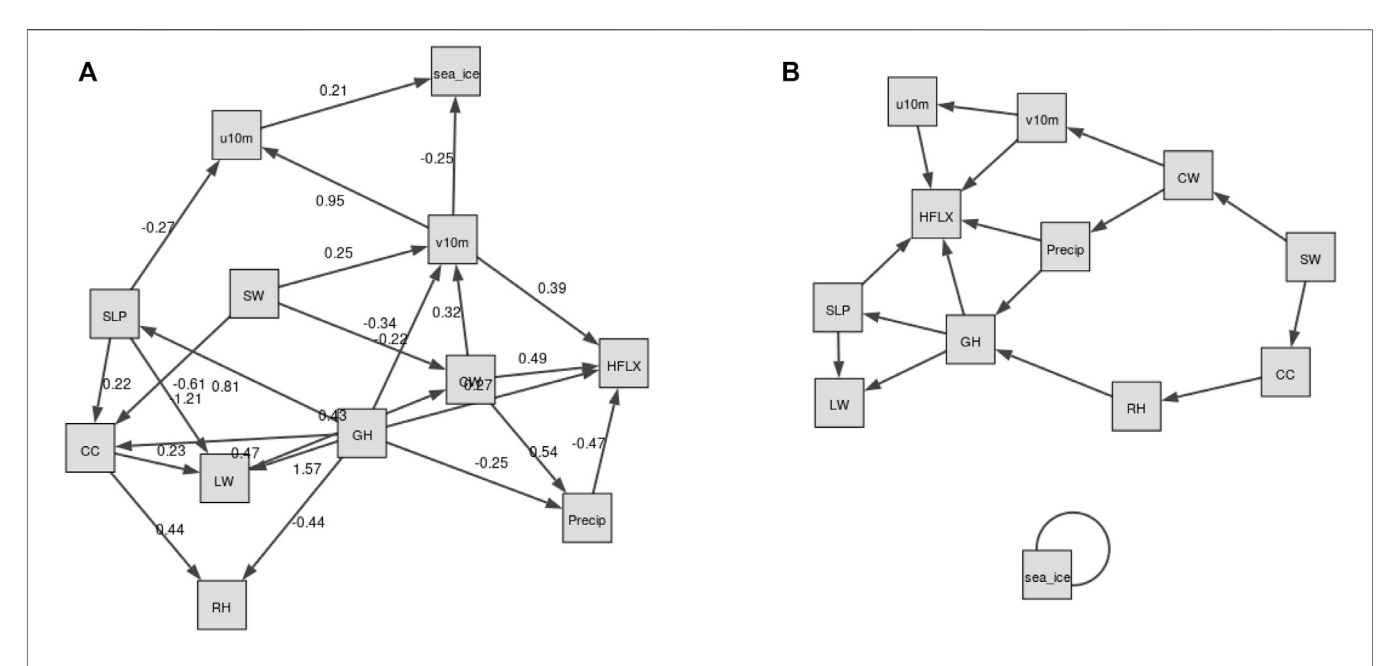


FIGURE 8 | The DAG-GNN graphs that are closest to the domain knowledge graph of **Figure 1. (A)**: The static graph for $\tau = 0$, t = 0.2. The larger weights indicate stronger connection between two variables. **(B)**: The temporal graph for $\tau \in \{0, e - 7\}$, t = 0.3.

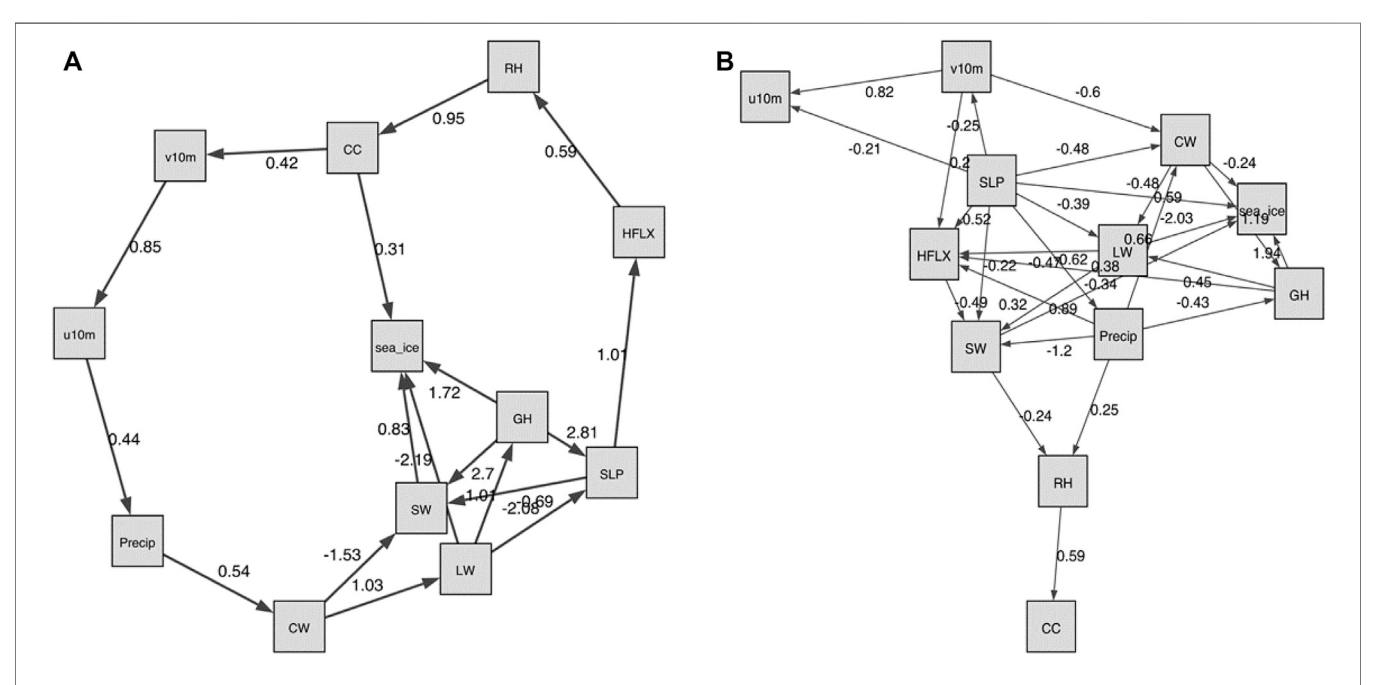


FIGURE 9 | The graphs produced with raw data sets (non-detrended and non-deseasonalized). **(A)**: The NOTEARS static graph for $\lambda = 0$, t = 0.3. **(B)**: The DAG-GNN static graph for $\tau = 0$, t = 0.2.

and v10 m. These connections are relatively reasonable since we average those variables in a large domain. However, there is no edge between sea ice and atmospheric components anymore. We believe that the connections between sea ice and atmosphere could have been filtered out, because the edges among atmospheric components have much larger weights.

6 CONCLUSION AND DISCUSSION

The Arctic has undergone dramatic changes in the past few decades, and sea ice decline is believed to be a key driver for the Arctic amplification. On the one hand, the sea ice is melted by mixed effects of atmospheric dynamical and thermodynamical

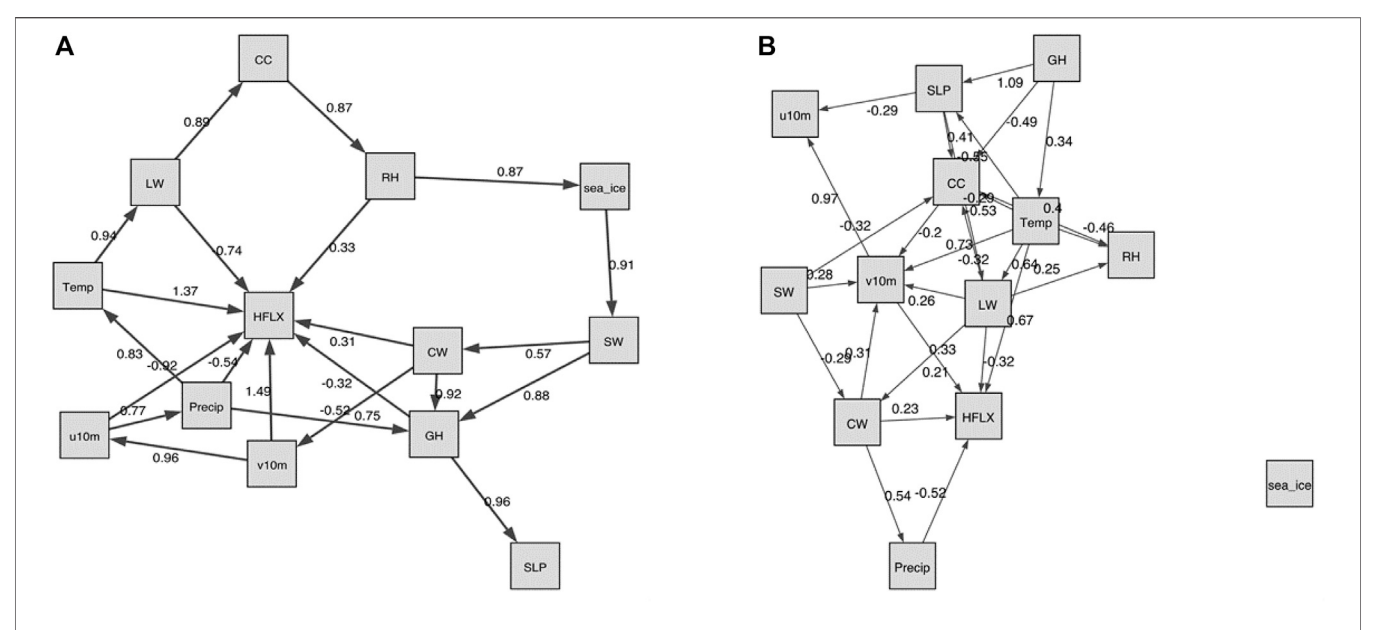


FIGURE 10 The graphs produced with data sets including air temperature averaged from 1,000 to 300 hPa. **(A)**: The NOTEARS static graph for $\lambda = 0$, t = 0.3. **(B)**: The DAG-GNN static graph for $\tau = 0$, t = 0.2.

processes. These processes on the other hand, can be largely affected by sea ice melt. Therefore, this study investigates the causality between multiple atmospheric processes and sea ice variations using three data-driven causality discovery approaches (TCDF, NOTEARS and DAG-GNN). As shown in previous sections, one advantage of utilizing these approaches is that they not only generate causal graphs, but also provide quantified information on causal strength through weights or time lags. Another advantage is that these approaches can take all relevant variables into consideration and find potentially important causal relationships, which is different from most related studies which only analyze pair-wise causality between two variables. Instead of performing computationally expensive climate model simulations, here we focus solely on an observational-based analysis. Specifically, we examine the sensitivity of causality graphs produced by three methods to different hyperparameters and then compare those graphs with domain knowledge graph.

We found that the outputs of the three algorithms are rather sensitive to the choice of hyperparameters. For example, choosing an only slightly too large regularization parameter can result in NOTEARS or DAG-GNN producing empty graphs, that is not discovering any causal relationships at all. Also the values of the other parameters turned out to be important and outputs for different choices of the hyperparameters can be quite different. Hence, some care must be taken when applying data-driven causality discovery approaches and domain knowledge is indispensable for assessing whether their produced outputs are reasonable.

Compared to domain knowledge graph, the static graphs produced by NOTEARS and DAG-GNN are relatively reasonable. The results from NOTEARS suggest that RH and precipitation dominate sea ice changes among all variables. In the

meantime, the sea ice has a large impact on SW and CW. The graph generated by DAG-GNN, however, indicates that the zonal (u10 m) and meridional (v10 m) wind fields are more important for driving sea ice variations than other variables. And there are no atmospheric variables being affected by the sea ice. Note that the edges between u10 m and v10 m, SW and v10 m, CW and v10 m are produced by both NOTEARS and DAG-GNN, which are different from domain knowledge graph, possibly due to the averages over a large domain. As for the temporal graphs, very few edges can be found in TCDF and NOTEARS. In comparison, the DAG-GNN is able to produce more complicated and meaningful results. The sea ice is found to have a delayed impact on itself, but with no causal relationship with any atmospheric processes. This is possibly because sea ice anomaly persistence is much stronger than the connections between sea ice and atmosphere. It is our hope that those causality graphs can be compared with the ones produced by other algorithms as Artificial Intelligence technologies are evolving rapidly. In the meantime, they can be also compared with the causal links captured by physical models for crossvalidation.

Based on our analysis, it is still very challenging to directly apply these state-of-the-art data-driven causality discovery approaches to this specific climate topic. However, there are several limitations with current study, which potentially has a large influence on our results. 1) There are large uncertainties in the domain knowledge graph and thus cannot be considered as ground truth. Climate scientists strive to investigate the complex feedbacks between atmosphere and sea ice, but our knowledge in this field is still very limited and controversial. For example, a few recent studies have divergent consensuses on Arctic amplification's influence on mid-latitude severe winter weather (Blackport et al., 2019; Cohen et al., 2019). 2) We average the

atmospheric and sea ice variables within the pan-Arctic domain (north of 60°N) and our analysis is only based on the time-series. However, the causal relationships between atmosphere and sea ice could be regionally dependent. 3) We use the full monthly atmosphere and sea ice records during 1980-2018. The feedbacks between atmosphere and sea ice are highly variable with season, and physical mechanisms work differently with and without sunlight. For example, previous studies pointed out the cloud response to sea ice melt occurs in all seasons except in summer (Kay and Gettelman, 2009; Taylor et al., 2015; Morrison et al., 2018; Huang et al., 2019a). Moreover, the interactions between atmosphere and sea ice may occur at shorter time scales (e.g., daily). 4) The weights among different atmospheric variables are much higher than those between atmosphere and sea ice. Thus, the edges in the latter category could have been filtered out. 6) We only consider the interactions between atmosphere and sea ice in this study. The oceanic processes (e.g., ocean currents, ocean salinity) might also exert large influence on sea ice variations in the Arctic. For example, when salt is ejected into the ocean as sea ice forms, the water's salinity increases. Therefore, a gradual freshening of the upper Arctic ocean will continue with Arctic sea ice decline (Li and Fedorov, 2021). Our study is a starting point to investigate the atmosphere-sea ice feedback using data-driven causality approaches, and it can be extended to the interactions between atmosphere, ocean, sea ice and even other components (e.g., land ice) in the future. 7) Only one global reanalysis product is used in this study and the results could be more robust if we expand our analysis with different products. It should be noted that the majority of connections considered in this study have been validated by different observational, reanalysis and/or climate models (Ding et al., 2017; Baxter et al., 2019). Thus, we believe that our results may not highly depend on the choice of data sets. Moreover, all results shown in this study are based on detrended and deseasonalized data. We also performed additional experiments with raw data. Based on NOTEARS and DAG-GNN, geopotential heights, clouds, surface longwave, and shortwave flux are found to dominate sea ice changes, which are different from the results shown in Figures 7, 8.

Nevertheless, this is a pioneer study in the application of data-drive causality discovery approaches in the interactions between atmosphere and sea ice. This study will pave the way for us to disentangle the complicated causal relationships in the Earth system, by taking the advantage of cutting-edge data science and Artificial Intelligence technologies. It also provides a good opportunity for climate scientists, data scientists and computer scientists to work together to solve the puzzle in the nature, which will eventually advance our understanding of polar climate system and global climate change.

REFERENCES

Aragam, B., Amini, A., and Zhou, Q. (2017). Learning Directed Acyclic Graphs with Penalized Neighbourhood Regression. ArXiv preprint. ArXiv:1511.08963.
 Baxter, I., Ding, Q., Schweiger, A., L'Heureux, M., Baxter, S., Wang, T., et al. (2019).
 How Tropical Pacific Surface Cooling Contributed to Accelerated Sea Ice Melt

DATA AVAILABILITY STATEMENT

The sea ice concentration and extent was obtained from the National Snow and Ice Data Center: http://nsidc.org/data/NSIDC-0051. The ECMWF ERA-5 global reanalysis product can be found via https://cds.climate.copernicus.eu/cdsapp#!/home. The codes and input for three models are available on GitHub: https://github.com/big-data-lab-umbc/cybertraining/tree/master/year-3-projects/team-6.

AUTHOR CONTRIBUTIONS

YH downloaded data sets, carried out data pre-processing, prepared the domain knowledge graph and wrote the paper; MK, AM, and DV implemented the causal discovery methods, generated their graphs and wrote the paper; PG carried out data pre-processing, worked on attention based causality discovery and dealt with technical issues related to high performance computing; JW provided direction to the project and crucial guidance for this work; All authors participated in regular constructive discussions and contributed to interpreting the results and writing the paper.

FUNDING

This work is supported by the grant "CyberTraining: DSE: Cross-Training of Researchers in Computing, Applied Mathematics and Atmospheric Sciences using Advanced Cyberinfrastructure Resources" (OAC–1730250) and grant "CAREER: Big Data Climate Causality Analytics" (OAC–1942714) from the National Science Foundation.

ACKNOWLEDGMENTS

The hardware used in the computational studies is part of the UMBC High Performance Computing Facility (HPCF). The facility is supported by the United States National Science Foundation through the MRI program (Grant Nos. CNS-0821258, CNS-1228778, and OAC-1726023) and the SCREMS program (Grant Nos. DMS-0821311), with additional substantial support from the University of Maryland, Baltimore County (UMBC). See hpcf.umbc.edu for more information on HPCF and the projects using its resources.

This manuscript has been released as a report at the UMBC High Performance Computing Facility (HPCF) web site (Huang et al. (2020).

from 2007 to 2012 as Ice Is Thinned by Anthropogenic Forcing. *J. Clim.* 32, 8583–8602. doi:10.1175/jcli-d-18-0783.1

Bintanja, R., and Selten, F. M. (2014). Future Increases in Arctic Precipitation Linked to Local Evaporation and Sea-Ice Retreat. *Nature* 509, 479–482. doi:10.1038/nature13259

Blackport, R., Screen, J. A., van der Wiel, K., and Bintanja, R. (2019). Minimal Influence of Reduced Arctic Sea Ice on Coincident Cold

winters in Mid-latitudes. Nat. Clim. Chang. 9, 697–704. doi:10.1038/s41558-019-0551-4

- Boisvert, L. N., and Stroeve, J. C. (2015). The Arctic Is Becoming Warmer and Wetter as Revealed by the Atmospheric Infrared Sounder. *Geophys. Res. Lett.* 42, 4439–4446. doi:10.1002/2015gl063775
- Boisvert, L. N., Wu, D., and Shie, C. (2015). Increasing Evaporation Amounts Seen in the Arctic between 2003 and 2013 from AIRS Data. J. Geophys. Res. Atmospheres 120, 6865–6881. doi:10.1002/2015jd023258
- Boisvert, L., Webster, M., Petty, A., Markus, T., Bromwich, D., and Cullather, R. (2018). Intercomparison of Precipitation Estimates over the Arctic Ocean and its Peripheral Seas from Reanalyses. J. Clim. 31, 8441–8462. doi:10.1175/jcli-d-18-0125.1
- Brockwell, P. J., Brockwell, P. J., Davis, R. A., and Davis, R. A. (2016). *Introduction to Time Series and Forecasting*. Springer.
- Cavalieri, D., Crawford, J., Drinkwater, M., Emery, W., Eppler, D., Farmer, L., et al. (1992). "NASA Sea Ice Validation Program for the DMSP SSM/I: Final Report, NASA Technical Memorandum 104559," in *Tech. Rep* (Washington, D.C.: National Aeronautics and Space Administration).
- Cavalieri, D., Parkinson, C., Gloersen, P., and Zwally, H. (1996). Sea Ice Concentrations from Nimbus-7 SMMR and DMSP SSM/I-SSMIS Passive Microwave Data, Version 1 (Boulder, CO, United States: NASA National Snow and Ice Data Center Distributed Active Archive Center). doi:10.5067/ 8GQ8LZQVL0VL
- Chemke, R., Polvani, L., and Deser, C. (2019). The Effect of Arctic Sea Ice Loss on the Hadley Circulation. *Geophys. Res. Lett.* 46, 963–972. doi:10.1029/ 2018gl081110
- Chickering, D. (1996). Learning Bayesian Networks Is NP-Complete. In *Learning from Data* (Springer), Vol. 112 of Lecture Notes in Statisticsdoi:10.1007/978-1-4612-2404-4 12
- Choi, Y., Kim, B., Hur, S., Kim, S., Kim, J., and Ho, C. (2014). Connecting Early Summer Cloud-Controlled Sunlight and Late Summer Sea Ice in the Arctic. J. Geophys. Res. Atmospheres 119, 11,087–11,099. doi:10.1002/2014jd022013
- Chu, T., Danks, D., and Glymour, C. (2005). "Data Driven Methods for Nonlinear Granger Causality: Climate Teleconnection Mechanisms," in *Tech. Rep. CMU-PHIL-171* (Department of Philosophy, Carnegie Mellon University).
- Chu, T., and Glymour, C. (2008). Search for Additive Nonlinear Time Series Causal Models. J. Machine Learn. Res. 9, 967–991. doi:10.5555/1390681.1390713
- Cohen, J., Screen, J., Furtado, J., Barlow, M., Whittleston, D., Coumou, D., et al. (2014). Recent Arctic Amplification and Extreme Mid-latitude Weather. *Nat. Geosci* 7, 627–637. doi:10.1038/ngeo2234
- Cohen, J., Zhang, X., Francis, J., Jung, T., Kwok, R., Overland, J., et al. (2019). Divergent Consensuses on Arctic Amplification Influence on Midlatitude Severe winter Weather. Nat. Clim. Change 10, 20–29. doi:10.1038/s41558-019-0662-y
- Cox, C. J., Uttal, T., Long, C. N., Shupe, M. D., Stone, R. S., and Starkweather, S. (2016). The Role of Springtime Arctic Clouds in Determining Autumn Sea Ice Extent. J. Clim. 29, 6581–6596. doi:10.1175/jcli-d-16-0136.1
- Cruz-García, R., Guemas, V., Chevallier, M., and Massonnet, F. (2019). An Assessment of Regional Sea Ice Predictability in the Arctic Ocean. Clim. Dyn. 53, 427–440. doi:10.1007/s00382-018-4592-6
- Ding, Q., Schweiger, A., L'Heureux, M., Battisti, D. S., Po-Chedley, S., Johnson, N. C., et al. (2017). Influence of High-Latitude Atmospheric Circulation Changes on Summertime Arctic Sea Ice. *Nat. Clim Change* 7, 289–295. doi:10.1038/nclimate3241
- Donnat, C., and Holmes, S. (2018). Tracking Network Dynamics: A Survey Using Graph Distances. *Ann. Appl. Stat.* 12, 971–1012. doi:10.1214/18-aoas1176
- Ebert-Uphoff, I., and Deng, Y. (2012). Causal Discovery for Climate Research Using Graphical Models. J. Clim. 25, 5648–5665. doi:10.1175/jcli-d-11-00387.1
- Entner, D., and Hoyer, P. O. (2010). "On Causal Discovery from Time Series Data Using FCI," in Proceedings of the Fifth European Workshop on Probabilistic Graphical Models, Helsinki, Finland. Editors P. Myllymaeki, T. Roos, and T. Jaakkola (HIIT Publications, 2010), 121–128.
- Eveleigh, V. W. (1967). "McGraw-Hill Electrical and Electronic Engineering Series," in Adaptive Control and Optimization Techniques (New York: McGraw-Hill).
- Graham, R. M., Cohen, L., Ritzhaupt, N., Segger, B., Graversen, R. G., Rinke, A., et al. (2019). Evaluation of Six Atmospheric Reanalyses over Arctic Sea Ice from winter to Early Summer. J. Clim. 32, 4121–4143. doi:10.1175/jcli-d-18-0643.1

Granger, C. W. J. (1969). Investigating Causal Relations by Econometric Models and Cross-Spectral Methods. *Econometrica* 37, 424–438. doi:10.2307/1912791

- Guemas, V., Blanchard-Wrigglesworth, E., Chevallier, M., Day, J. J., Déqué, M., Doblas-Reyes, F. J., et al. (2016). A Review on Arctic Sea-Ice Predictability and Prediction on Seasonal to Decadal Time-Scales. Q.J.R. Meteorol. Soc. 142, 546–561. doi:10.1002/gi.2401
- Guo, R., Cheng, L., Li, J., Hahn, P. R., and Liu, H. (2020). A Survey of Learning Causality with Data: Problems and Methods. ACM Computing Surveys (CSUR) 53, 1–37. doi:10.1145/3397269
- Hamilton, J. D. (1994). Time Series Analysis. Princeton University Press.
- Heckerman, D., Geiger, D., and Chickering, D. M. (1995). Learning Bayesian Networks: The Combination of Knowledge and Statistical Data. *Mach Learn*. 20, 197–243. doi:10.1007/bf00994016
- Hersbach, H., Bell, B., Berrisford, P., Hirahara, S., Horányi, A., Muñoz-Sabater, J., et al. (2020). The ERA5 Global Reanalysis. Q. J. R. Meteorol. Soc. 146, 1999–2049. doi:10.1002/qj.3803
- Hochreiter, S. (1998). The Vanishing Gradient Problem during Learning Recurrent Neural Nets and Problem Solutions. Int. J. Unc. Fuzz. Knowl. Based Syst. 06, 107–116. doi:10.1142/s0218488598000094
- Holland, M. M., and Bitz, C. M. (2003). Polar Amplification of Climate Change in Coupled Models. Clim. Dyn. 21, 221–232. doi:10.1007/s00382-003-0332-6
- Holland, M. M., Landrum, L., Bailey, D., and Vavrus, S. (2019). Changing Seasonal Predictability of Arctic Summer Sea Ice Area in a Warming Climate. J. Clim. 32, 4963–4979. doi:10.1175/jcli-d-19-0034.1
- Huang, Y., Ding, Q., Dong, X., Xi, B., and Baxter, I. (2021). Summertime Low Clouds Mediate The Impact Of The Large-Scale Circulation On Arctic Sea Ice. Commun. Earth Environ. 2, 1–10. doi:10.1038/s43247-021-00114-w
- Huang, Y., Dong, X., Bailey, D. A., Holland, M. M., Xi, B., DuVivier, A. K., et al. (2019a). Thicker Clouds and Accelerated Arctic Sea Ice Decline: The Atmosphere-Sea Ice Interactions in Spring. Geophys. Res. Lett. 46, 6980–6989. doi:10.1029/2019gl082791
- Huang, Y., Dong, X., Xi, B., and Deng, Y. (2019b). A Survey of the Atmospheric Physical Processes Key to the Onset of Arctic Sea Ice Melt in spring. Clim. Dyn. 52, 4907–4922. doi:10.1007/s00382-018-4422-x
- Huang, Y., Dong, X., Xi, B., Dolinar, E. K., and Stanfield, R. E. (2017). The Footprints of 16 Year Trends of Arctic Springtime Cloud and Radiation Properties on September Sea Ice Retreat. J. Geophys. Res. Atmos. 122, 2179–2193. doi:10.1002/2016jd026020
- Huang, Y., Kleindessner, M., Munishkin, A., Varshney, D., Guo, P., and Wang, J. (2020). "Benchmarking of Data-Driven Causality Discovery Approaches in the Interactions of Arctic Sea Ice and Atmosphere," in *Technical Report HPCF-*2020-16, UMBC High Performance Computing Facility (Baltimore County: University of Maryland).
- Hussung, S., Mahmud, S., Sampath, A., Wu, M., Guo, P., and Wang, J. (2019).
 "Evaluation of Data-Driven Causality Discovery Approaches Among Dominant Climate Modes," in *Technical Report HPCF-2019-12*, *UMBC High Performance Computing Facility* (Baltimore County: University of Maryland).
- Iler, A. M., Inouye, D. W., Schmidt, N. M., and Høye, T. T. (2017). Detrending Phenological Time Series Improves Climate-Phenology Analyses and Reveals Evidence of Plasticity. *Ecology* 98, 647–655. doi:10.1002/ecy.1690
- Kapsch, M.-L., Graversen, R. G., Tjernström, M., and Bintanja, R. (2016). The Effect of Downwelling Longwave and Shortwave Radiation on Arctic Summer Sea Ice. J. Clim. 29, 1143–1159. doi:10.1175/jcli-d-15-0238.1
- Kapsch, M.-L., Graversen, R. G., and Tjernström, M. (2013). Springtime Atmospheric Energy Transport and the Control of Arctic Summer Sea-Ice Extent. Nat. Clim Change 3, 744–748. doi:10.1038/nclimate1884
- Kapsch, M.-L., Skific, N., Graversen, R. G., Tjernström, M., and Francis, J. A. (2019). Summers with Low Arctic Sea Ice Linked to Persistence of spring Atmospheric Circulation Patterns. Clim. Dyn. 52, 2497–2512. doi:10.1007/s00382-018-4279-z
- Kawale, J., Liess, S., Kumar, A., Steinbach, M., Snyder, P., Kumar, V., et al. (2013). A Graph-Based Approach to Find Teleconnections in Climate Data. Stat. Analy Data Mining 6, 158–179. doi:10.1002/sam.11181
- Kay, J. E., and Gettelman, A. (2009). Cloud Influence on and Response to Seasonal Arctic Sea Ice Loss. J. Geophys. Res. Atmospheres 114. doi:10.1029/ 2009jd011773

Kennel, C. F., and Yulaeva, E. (2020). Influence of Arctic Sea-Ice Variability on Pacific Trade Winds. Proc. Natl. Acad. Sci. USA 117, 2824–2834. doi:10.1073/ pnas.1717707117

- Kingma, D. P., and Welling, M. (2014). "Auto-Encoding Variational Bayes," in 2nd International Conference on Learning Representations, ICLR 2014. Conference Track Proceedings, Banff, AB, Canada, April 14-16, 2014. Editors Y. Bengio and Y. LeCun
- Kopec, B. G., Feng, X., Michel, F. A., and Posmentier, E. S. (2016). Influence of Sea Ice on Arctic Precipitation. *Proc. Natl. Acad. Sci. USA* 113, 46–51. doi:10.1073/ pnas.1504633113
- Kretschmer, M., Coumou, D., Donges, J. F., and Runge, J. (2016). Using Causal Effect Networks to Analyze Different Arctic Drivers of Midlatitude Winter Circulation. J. Clim. 29, 4069–4081. doi:10.1175/jcli-d-15-0654.1
- Lee, S., Gong, T., Feldstein, S. B., Screen, J. A., and Simmonds, I. (2017). Revisiting the Cause of the 1989–2009 Arctic Surface Warming Using the Surface Energy Budget: Downward Infrared Radiation Dominates the Surface Fluxes. *Geophys. Res. Lett.* 44, 10–654. doi:10.1002/2017gl075375
- Li, H., Fedorov, A., and Liu, W. (2021). AMOC stability and diverging response to Arctic sea ice decline in two climate models. J. Clim. 34, 5443–5460. doi:10.1175/jcli-d-20-0572.1
- Loh, P.-L., and Bühlmann, P. (2014). High-Dimensional Learning of Linear Causal Networks via Inverse Covariance Estimation. J. Machine Learn. Res. 15, 3065–3105.
- Luo, B., Luo, D., Wu, L., Zhong, L., and Simmonds, I. (2017). Atmospheric Circulation Patterns Which Promote winter Arctic Sea Ice Decline. *Environ. Res. Lett.* 12, 054017. doi:10.1088/1748-9326/aa69d0
- Luo, B., Wu, L., Luo, D., Dai, A., and Simmonds, I. (2019a). The winter Midlatitude-Arctic Interaction: Effects of North Atlantic SST and High-Latitude Blocking on Arctic Sea Ice and Eurasian Cooling. Clim. Dyn. 52, 2981–3004. doi:10.1007/s00382-018-4301-5
- Luo, D., Chen, X., Dai, A., and Simmonds, I. (2018). Changes in Atmospheric Blocking Circulations Linked with winter Arctic Warming: A New Perspective. J. Clim. 31, 7661–7678. doi:10.1175/jcli-d-18-0040.1
- Luo, D., Chen, X., Overland, J., Simmonds, I., Wu, Y., and Zhang, P. (2019b). Weakened Potential Vorticity Barrier Linked to Recent winter Arctic Sea Ice Loss and Midlatitude Cold Extremes. J. Clim. 32, 4235–4261. doi:10.1175/jcli-d-18-0449.1
- Luo, R., Ding, Q., Wu, Z., Baxter, L., Bushuk, M., Huang, Y., et al. (2021). Summertime Atmosphere-Sea Ice Coupling In The Arctic Simulated By CMIP5/6 Models: Importance Of Large-Scale Circulation. Clim. Dyn. 56, 1467–1485. doi:10.1007/s00382-020-05543-5
- Marcovecchio, A., Behrangi, A., Dong, X., Xi, B., and Huang, Y. (2021).
 Precipitation Influence on and Response to Early and Late Arctic Sea Ice
 Melt Onset During Melt Season. *Inter. J. Climatol.*, 1–16. doi:10.1002/joc.7233
- Matthewman, N. J., and Magnusdottir, G. (2011). Observed Interaction between Pacific Sea Ice and the Western Pacific Pattern on Intraseasonal Time Scales. *J. Clim.* 24, 5031–5042. doi:10.1175/2011jcli4216.1
- Mayer, M., Tietsche, S., Haimberger, L., Tsubouchi, T., Mayer, J., and Zuo, H. (2019). An Improved Estimate of the Coupled Arctic Energy Budget. J. Clim. 32, 7915–7934. doi:10.1175/jcli-d-19-0233.1
- McGraw, M. C., and Barnes, E. A. (2018). Memory Matters: A Case for Granger Causality in Climate Variability Studies. J. Clim. 31, 3289–3300. doi:10.1175/ jcli-d-17-0334.1
- Morrison, A., Kay, J., Chepfer, H., Guzman, R., and Yettella, V. (2018). Isolating the Liquid Cloud Response to Recent Arctic Sea Ice Variability Using Spaceborne Lidar Observations. J. Geophys. Res. Atmospheres 123, 473–490. doi:10.1002/ 2017jd027248
- Nauta, M., Bucur, D., and Seifert, C. (2019). "Causal Discovery with Attention-Based Convolutional Neural Networks," in *Machine Learning and Knowledge Extraction*, 1, 312–340. Code available on: https://github.com/M-Nauta/TCDF. doi:10.3390/make1010019
- Nocedal, J., and Wright, S. (2006). Numerical Optimization. Springer.
- Nussbaumer, E. A., and Pinker, R. T. (2012). The Role of Shortwave Radiation in the 2007 Arctic Sea Ice Anomaly. Geophys. Res. Lett. 39, L15808. doi:10.1029/ 2012gl052415
- Overland, J. E., and Wang, M. (2010). Large-scale Atmospheric Circulation Changes Are Associated with the Recent Loss of Arctic Sea Ice. Tellus A:

- Dynamic Meteorology and Oceanography 62, 1-9. doi:10.1111/j.1600-0870.2009.00421.x
- Overpeck, J. T., Meehl, G. A., Bony, S., and Easterling, D. R. (2011). Climate Data Challenges in the 21st Century. Science 331, 700–702. doi:10.1126/ science.1197869
- Parkinson, C., and Comiso, J. (2013). On the 2012 Record Low Arctic Sea Ice Cover: Combined Impact of Preconditioning and an August Storm. Geophys. Res. Lett. 40. doi:10.1002/grl.50349
- Perovich, D., Grenfell, T., Light, B., and Hobbs, P. (2002). Seasonal Evolution of the Albedo of Multiyear Arctic Sea Ice. *J. Geophys. Res. Oceans* 107, SHE20-1-SHE 20-13. doi:10.1029/2000jc000438
- [Dataset] Peters, J., Janzing, D., and Schölkopf, B. (2012). Causal Inference on Time Series Using Structural Equation Models. arXiv preprint. arXiv:1207.5136.
- Ramsey, J., Glymour, M., Sanchez-Romero, R., and Glymour, C. (2017). A Million Variables and More: the Fast Greedy Equivalence Search Algorithm for Learning High-Dimensional Graphical Causal Models, with an Application to Functional Magnetic Resonance Images. *Int. J. Data Sci. Anal.* 3, 121–129. doi:10.1007/s41060-016-0032-z
- Rinke, A., Knudsen, E., Mewes, D., Dorn, W., Handorf, D., Dethloff, K., et al. (2019). Arctic Summer Sea Ice Melt and Related Atmospheric Conditions in Coupled Regional Climate Model Simulations and Observations. J. Geophys. Res. Atmospheres 124, 6027–6039. doi:10.1029/2018jd030207
- Runge, J., Nowack, P., Kretschmer, M., Flaxman, S., and Sejdinovic, D. (2019). Detecting and Quantifying Causal Associations in Large Nonlinear Time Series Datasets. Sci. Adv. 5, eaau4996. doi:10.1126/sciadv.aau4996
- Samarasinghe, S., McGraw, M., Barnes, E., and Ebert-Uphoff, I. (2019). A Study of Links between the Arctic and the Midlatitude Jet Stream Using Granger and Pearl Causality. *Environmetrics* 30, e2540. doi:10.1002/env.2540
- Schmidhuber, J. (2015). Deep Learning in Neural Networks: An Overview. Neural networks 61, 85–117. doi:10.1016/j.neunet.2014.09.003
- Screen, J. A., Bracegirdle, T. J., and Simmonds, I. (2018). Polar Climate Change as Manifest in Atmospheric Circulation. *Curr. Clim. Change Rep.* 4, 383–395. doi:10.1007/s40641-018-0111-4
- Screen, J. A., and Simmonds, I. (2012). Declining Summer Snowfall in the Arctic: Causes, Impacts and Feedbacks. Clim. Dyn. 38, 2243–2256. doi:10.1007/s00382-011-1105-2
- Screen, J. A., Simmonds, I., and Keay, K. (2011). Dramatic Interannual Changes of Perennial Arctic Sea Ice Linked to Abnormal Summer Storm Activity. J. Geophys. Res. Atmospheres 116, D15105. doi:10.1029/2011jd015847
- Semmler, T., McGrath, R., and Wang, S. (2012). The Impact of Arctic Sea Ice on the Arctic Energy Budget and on the Climate of the Northern Mid-latitudes. *Clim. Dyn.* 39, s–2694. doi:10.1007/s00382-012-1353-9
- Serreze, M. C., and Stroeve, J. (2015). Arctic Sea Ice Trends, Variability and Implications for Seasonal Ice Forecasting. *Philos. Trans. A. Math. Phys. Eng. Sci.* 373, 20140159. doi:10.1098/rsta.2014.0159
- Serreze, M. C., and Barry, R. G. (2011). Processes and Impacts of Arctic Amplification: A Research Synthesis. Glob. Planet. Change 77, 85–96. doi:10.1016/j.gloplacha.2011.03.004
- Simmonds, I., Burke, C., and Keay, K. (2008). Arctic Climate Change as Manifest in Cyclone Behavior. *J. Clim.* 21, 5777–5796. doi:10.1175/2008jcli2366.1
- Simmonds, I. (2015). Comparing and Contrasting the Behaviour of Arctic and Antarctic Sea Ice over the 35 Year Period 1979-2013. Ann. Glaciol. 56, 18–28. doi:10.3189/2015aog69a909
- Simmonds, I., and Govekar, P. D. (2014). What Are the Physical Links between Arctic Sea Ice Loss and Eurasian winter Climate?. Environ. Res. Lett. 9, 101003. doi:10.1088/1748-9326/9/10/101003
- Simmonds, I., and Keay, K. (2009). Extraordinary September Arctic Sea Ice Reductions and Their Relationships with Storm Behavior over 1979–2008. Geophys. Res. Lett. 36, L19715. doi:10.1029/2009gl039810
- Simmonds, I., and Rudeva, I. (2014). A Comparison of Tracking Methods for Extreme Cyclones in the Arctic basin. Tellus A: Dynamic Meteorology and Oceanography 66, 25252. doi:10.3402/tellusa.v66.25252
- Simmonds, I., and Rudeva, I. (2012). The Great Arctic Cyclone of August 2012. Geophys. Res. Lett. 39, n/a. doi:10.1029/2012gl054259
- Song, H., Tian, J., Huang, J., Guo, P., Zhang, Z., and Wang, J. (2019). Hybrid Causality Analysis of ENSO's Global Impacts on Climate Variables Based on Data-Driven Analytics and Climate Model Simulation. Front. Earth Sci. 7, 233. doi:10.3389/feart.2019.00233

Song, H., Wang, J., Tian, J., Huang, J., and Zhang, Z. (2018). "Spatio-Temporal Climate Data Causality Analytics-An Analysis of ENSO's Global Impacts," in Proceedings of the 8th International Workshop on Climate Informatics (CI2018), Boulder, CO, United States, September 19–21, 2018, 45–48.

- Spreen, G., Kwok, R., and Menemenlis, D. (2011). Trends in Arctic Sea Ice Drift and Role of Wind Forcing: 1992–2009. Geophys. Res. Lett. 38. doi:10.1029/ 2011gl048970
- Stocker, T., Qin, D., Plattner, G.-K., Alexander, L., Allen, S., Bindoff, N., et al. (2013). Technical Summary. Cambridge, United Kingdom and New York, NY, USA: Cambridge University Press, 33–115. book section TS. doi:10.1017/ CBO9781107415324.005
- Strong, C., Magnusdottir, G., and Stern, H. (2009). Observed Feedback between Winter Sea Ice and the North Atlantic Oscillation. J. Clim. 22, 6021–6032. doi:10.1175/2009jcli3100.1
- Sturm, M., Holmgren, J., and Perovich, D. K. (2002). Winter Snow Cover on the Sea Ice of the Arctic Ocean at the Surface Heat Budget of the Arctic Ocean (SHEBA): Temporal Evolution and Spatial Variability. J. Geophys. Res. Oceans 107, SHE 23-1-SHE 23-17. doi:10.1029/2000jc000400
- Sun, L., Perlwitz, J., and Hoerling, M. (2016). What Caused the Recent "Warm Arctic, Cold Continents" Trend Pattern in Winter Temperatures? *Geophys. Res. Lett.* 43, 5345–5352. doi:10.1002/2016gl069024
- Tan, H. H., and Lim, K. H. (2019). "Vanishing Gradient Mitigation with Deep Learning Neural Network Optimization," in 2019 7th International Conference on Smart Computing & Communications (ICSCC), Sarawak, Malaysia, June 28–30, 2019 (IEEE), 1–4. doi:10.1109/icscc.2019.8843652
- Taylor, P. C., Kato, S., Xu, K. M., and Cai, M. (2015). Covariance between Arctic Sea Ice and Clouds within Atmospheric State Regimes at the Satellite Footprint Level. J. Geophys. Res. Atmos. 120, 12656–12678. doi:10.1002/2015jd023520
- Topál, D., Ding, Q., Mitchell, J., Baxter, I., Herein, M., Haszpra, T., et al. (2020). An Internal Atmospheric Process Determining Summertime Arctic Sea Ice Melting in the Next Three Decades: Lessons Learned from Five Large Ensembles and Multiple CMIP5 Climate Simulations. J. Clim. 33, 7431–7454. doi:10.1175/jclid-19-0803.1
- Van de Geer, S., and Bühlmann, P. (2013). l₀-penalized Maximum Likelihood for Sparse Directed Acyclic Graphs. Ann. Stat. 41, 536–567. doi:10.1214/13aos1085
- Wang, C., Graham, R., Wang, K., Gerland, S., and Granskog, M. (2019). Comparison of ERA5 and ERA-Interim Near-Surface Air Temperature, Snowfall and Precipitation over Arctic Sea Ice: Effects on Sea Ice Thermodynamics and Evolution. *The Cryosphere* 13, 1661–1679. doi:10.5194/tc-13-1661-2019
- Wang, J., Zhang, J., Watanabe, E., Ikeda, M., Mizobata, K., Walsh, J. E., et al. (2009). Is the Dipole Anomaly a Major Driver to Record Lows in Arctic Summer Sea Ice Extent?. Geophys. Res. Lett. 36, L05706. doi:10.1029/2008gl036706
- Watanabe, E., Wang, J., Sumi, A., and Hasumi, H. (2006). Arctic Dipole Anomaly and its Contribution to Sea Ice export from the Arctic Ocean in the 20th century. Geophys. Res. Lett. 33, L23703. doi:10.1029/2006gl028112
- Weber, R. O., and Talkner, P. (2001). Spectra and Correlations of Climate Data from Days to Decades. J. Geophys. Res. 106, 20131–20144. doi:10.1029/ 2001jd000548

- Wei, Q. (2018). "Self-Learning Optimal Control of Nonlinear Systems: Adaptive Dynamic Programming Approach," in Studies in Systems, Decision and Control (Singapore: Springer Singapore), 103.
- Wu, B., Overland, J., and D'Arrigo, R. (2012). Anomalous Arctic Surface Wind Patterns and Their Impacts on September Sea Ice Minima and Trend. Tellus A: Dynamic Meteorology and Oceanography 64, 18590. doi:10.3402/tellusa.v64i0.18590
- Wu, Z., Huang, N. E., Long, S. R., and Peng, C.-K. (2007). On the Trend, Detrending, and Variability of Nonlinear and Nonstationary Time Series. Proc. Natl. Acad. Sci. 104, 14889–14894. doi:10.1073/pnas.0701020104
- Yao, Y., Luo, D., Dai, A., and Simmonds, I. (2017). Increased Quasi Stationarity and Persistence of winter Ural Blocking and Eurasian Extreme Cold Events in Response to Arctic Warming. Part I: Insights from Observational Analyses. J. Clim. 30, 3549–3568. doi:10.1175/jcli-d-16-0261.1
- Yin, W., Schütze, H., Xiang, B., and Zhou, B. (2016). ABCNN: Attention-Based Convolutional Neural Network for Modeling Sentence Pairs. *Tacl.* 4, 259–272. doi:10.1162/tacl_a_00097
- Yu, Y., Chen, J., Gao, T., and Yu, M. (2019). "DAG-GNN: DAG Structure Learning with Graph Neural Networks," in Proceedings of the 36th International Conference on Machine Learning, Long Beach, CA, United States, June 9–15, 2019. Code available on: https://github.com/fishmoon1234/DAG-GNN.
- Zerenner, T., Friederichs, P., Lehnertz, K., and Hense, A. (2014). A Gaussian Graphical Model Approach to Climate Networks. Chaos 24, 023103. doi:10.1063/1.4870402
- Zhang, K., Schölkopf, B., Spirtes, P., and Glymour, C. (2018). Learning Causality and Causality-Related Learning: Some Recent Progress. *Natl. Sci. Rev.* 5, 26–29. doi:10.1093/nsr/nwx137
- Zhang, X., He, J., Zhang, J., Polyakov, I., Gerdes, R., Inoue, J., et al. (2013).
 Enhanced Poleward Moisture Transport and Amplified Northern HighLatitude Wetting Trend. Nat. Clim Change 3, 47–51. doi:10.1038/nclimate1631
- Zheng, X., Aragam, B., Ravikumar, P., and Xing, E. (2018). "DAGs with NO TEARS: Continuous Optimization for Structure Learning," in Conference on Neural Information Processing Systems, Montréal, Canada, December 2–8, 2018. (NeurIPS). Code available on: https://github.com/xunzheng/notears.

Conflict of Interest: The authors declare that the research was conducted in the absence of any commercial or financial relationships that could be construed as a potential conflict of interest.

Publisher's Note: All claims expressed in this article are solely those of the authors and do not necessarily represent those of their affiliated organizations, or those of the publisher, the editors and the reviewers. Any product that may be evaluated in this article, or claim that may be made by its manufacturer, is not guaranteed or endorsed by the publisher.

Copyright © 2021 Huang, Kleindessner, Munishkin, Varshney, Guo and Wang. This is an open-access article distributed under the terms of the Creative Commons Attribution License (CC BY). The use, distribution or reproduction in other forums is permitted, provided the original author(s) and the copyright owner(s) are credited and that the original publication in this journal is cited, in accordance with accepted academic practice. No use, distribution or reproduction is permitted which does not comply with these terms.